Journal of Hydrology 538 (2016) 726–742

Contents lists available at ScienceDirect

Journal of Hydrology

journal homepage: www.elsevier.com/locate/jhydrol

Contributions of human activities to suspended sediment yield during storm events from a small, steep, tropical watershed

A.M. Messina *, T.W. Biggs [1]

San Diego State University, Department of Geography, San Diego, CA 92182, USA

ARTICLE INFO

Article history:
Received 7 December 2015
Received in revised form 9 March 2016
Accepted 22 March 2016
Available online 15 April 2016
This manuscript was handled by Tim R. McVicar, Editor-in-Chief, with the assistance of Patrick Norman Lane, Associate Editor

Keywords:
Suspended sediment yield
Volcanic islands
Land use
Storm events
Coastal sediment yield
American Samoa

SUMMARY

Suspended sediment concentrations (SSC) and yields (SSY) were measured during storm and non-storm periods from undisturbed and human-disturbed portions of a small (1.8 km^2), mountainous watershed that drains to a sediment-stressed coral reef. Event-wise SSY (SSY_{EV}) was calculated for 142 storms from measurements of water discharge (Q), turbidity (T), and SSC measured downstream of three key sediment sources: undisturbed forest, an aggregate quarry, and a village. SSC and SSY_{EV} were significantly higher downstream of the quarry during both storm- and non-storm periods. The human-disturbed subwatershed (10.1% disturbed) accounted for an average of 87% of SSY_{EV} from the watershed. Observed sediment yield (mass) to the coast, including human disturbed subwatersheds, was 3.9× the natural background. Specific SSY (mass/area) from the disturbed quarry area was 49× higher than from natural forest compared with 8× higher from the village area. Similar to mountainous watersheds in semi-arid and temperate climates, SSY_{EV} from both the undisturbed and disturbed watersheds correlated closely with maximum event discharge (Q_{max}), event total precipitation and event total Q, but not with the Erosivity Index. Best estimates of annual SSY varied by method, from 45 to 143 tons/km^2/yr from the undisturbed subwatershed, 441–598 tons/km^2/yr from the human-disturbed subwatershed, and 241–368 tons/km^2/yr from the total watershed. Sediment yield was very sensitive to disturbance; the quarry covers 1.1% of the total watershed area, but contributed 36% of SSY_{EV}. Given the limited access to gravel for infrastructure development, sediment disturbance from local aggregate mining may be a critical sediment source on remote islands in the Pacific and elsewhere. Identification of erosion hotspots like the quarry using rapid, event-wise measures of suspended sediment yield will help efforts to mitigate sediment stress and restore coral reefs.

1. Introduction

Human disturbances including deforestation, agriculture, roads, mining, and urbanization alter the timing, composition, and amount of sediment loads to downstream ecosystems (Syvitski et al., 2005). Increased sediment yields can stress aquatic ecosystems downstream of impacted watersheds, including coral reefs, by decreasing light for photosynthesis and increasing sediment accumulation rates (Fabricius, 2005; Storlazzi et al., 2015). Anthropogenic sediment disturbance can be particularly high on volcanic islands in the humid tropics, where erosion potential is high due to high rainfall and steep slopes (Milliman and Syvitski, 1992). The steep topography and small floodplains on small volcanic islands limits sediment storage and the buffering capacity of the watershed against increased hillslope sediment supply (Walling, 1999). Such environments characterize many volcanic islands in the South Pacific and elsewhere where many coral reefs are sediment-stressed (Bégin et al., 2014; Fallon et al., 2002; Hettler et al., 1997; Rotmann and Thomas, 2012).

A large proportion of sediment yield can originate from disturbances that cover small fractions of the watershed area, suggesting management should focus on erosion hotspots. In the grazing-disturbed Kawela watershed on Molokai, Hawaii, most of the sediment originated from less than 5% of the watershed area, and 50% of the sediment originated from only 1% of the watershed (Risk, 2014; Stock et al., 2010). On St. John in the Caribbean, unpaved roads covering 0.3–0.9% of the watershed were the dominant sediment source, and increased sediment yield to the coast by 5–9× relative to undisturbed watersheds (Ramos-Scharrón and Macdonald, 2007). In the U.S. Pacific Northwest, most road-generated sediment originated from just a small fraction of

* Corresponding author. Tel.: +1 619 594 5437.
E-mail addresses: amessina@rohan.sdsu.edu (A.M. Messina), tbiggs@mail.sdsu.edu (T.W. Biggs).
[1] Tel.: +1 619 594 0902.

http://dx.doi.org/10.1016/j.jhydrol.2016.03.053
0022-1694/

unpaved roads (Gomi et al., 2005; Henderson and Toews, 2001; Megahan et al., 2001; Wemple et al., 1996), and heavily used roads yielded 130× as much sediment as abandoned roads (Reid and Dunne, 1984).

Sediment management requires linking changes in land use to changes in sediment yields at the watershed outlet (Walling and Collins, 2008). A sediment budget quantifies sediment movement from key sources like hillslope erosion, channel-bank erosion, and mass movements, to its eventual exit from a watershed (Rapp, 1960). Walling (1999) used a sediment budget to show that sediment yield from watersheds can be insensitive to both land use change and erosion management due to high sediment storage capacity on hillslopes and in the channel. Sediment yield from disturbed areas can also be large but relatively unimportant compared to high yields from undisturbed areas. The sediment budget can be simplified since most applications require only the order of magnitude or relative importance of processes be known (Slaymaker, 2003). Reid and Dunne (1996) argue a management-focused sediment budget can be developed quickly where the problem is clearly defined and the management area can be divided into homogenous sub-units.

Knowledge of suspended sediment yield (SSY) under both natural and disturbed conditions on most tropical, volcanic islands remains limited, due to the challenges of in situ monitoring in remote environments. Existing erosion models are mainly designed for agricultural landscapes, which are not well-calibrated to the physical geography of steep, tropical islands, and ignore important processes like mass movements (Calhoun and Fletcher, 1999; Ramos-Scharrón and Macdonald, 2005; Sadeghi et al., 2007). Models that predict SSY from small, mountainous catchments would establish baselines for change-detection, and improve regional-scale sediment yield models (Duvert et al., 2012).

Traditional approaches to quantifying human impact on sediment budgets include comparison of total annual yields (Fahey et al., 2003) and sediment rating curves (Asselman, 2000; Walling, 1977). These approaches are complicated by interannual climatic variability and hysteresis in the discharge-sediment concentration relationship (Ferguson et al., 1991; Gray et al., 2014; Kostaschuk et al., 2002; Stock and Tribble, 2010). Sediment yield can be highly variable over various time scales, even under natural conditions. At geologic time scales, sediment yield from a disturbed watershed may decrease as it reaches steady-state, or sediment contributions from subwatersheds may change with time (Ferrier et al., 2013; Perroy et al., 2012). At decadal scales, cyclical climatic patterns like El Nino-Southern Oscillation events or Pacific Decadal Oscillation can significantly alter sediment yield from undisturbed watersheds (Wulf et al., 2012).

SSY generated by storm events of the same magnitude can be used to compare the contribution of subwatersheds to total SSY (Zimmermann et al., 2012), determine temporal changes in SSY (Bonta, 2000), and relate SSY to various precipitation or discharge variables ("storm metrics") (Basher et al., 2011; Duvert et al., 2012; Fahey et al., 2003; Hicks, 1990). The relative anthropogenic impact on SSY_{EV} may vary by storm magnitude, as documented in Pacific Northwest forests (Lewis et al., 2001). As storm magnitude increases, water yield and/or SSY_{EV} from natural areas may increase relative to human-disturbed areas, diminishing anthropogenic impact relative to the natural baseline. While large storms account for most SSY under undisturbed conditions, the disturbance ratio (DR) may be highest for small storms, when background SSY_{EV} from the undisturbed forest is low and erodible sediment from disturbed surfaces is the dominant source (Lewis et al., 2001). For large storms, mass movements and bank erosion in undisturbed areas can increase the natural background and reduce the DR for large events.

Event-wise SSY (SSY_{EV}) may correlate with storm metrics such as total precipitation, the Erosivity Index (EI) (Kinnell, 2013), or total discharge, but the best correlation has consistently been found with maximum event discharge (Q_{max}). The EI quantifies the erosive energy of rainfall. Several researchers have hypothesized that Q_{max} integrates the hydrological response of a watershed, making it a good predictor of SSY_{EV} in diverse environments (Duvert et al., 2012; Rankl, 2004). High correlation between SSY_{EV} and Q_{max} has been found in semi-arid, temperate, and sub-humid watersheds in Wyoming (Rankl, 2004), Mexico, Italy, France (Duvert et al., 2012), and New Zealand (Basher et al., 2011; Hicks, 1990), but this approach has not been attempted for steep, tropical watersheds on volcanic islands.

This study uses in situ measurements of precipitation (P), water discharge (Q), turbidity (T), and suspended sediment concentration (SSC) to accomplish three objectives and answer the following research questions:

(1) Quantify suspended sediment concentrations (SSC) and yields (SSY) at the outlets of undisturbed and human-disturbed portions of Faga'alu watershed during storm and non-storm periods. How does SSC vary between storm and non-storm periods? How much has human disturbance increased SSY during storm events? Which land uses dominate the anthropogenic contribution to SSY?
(2) Develop an empirical model to predict SSY_{EV} from easily-monitored discharge or precipitation metrics. Which storm metric is the best predictor of SSY_{EV}? How does human-disturbance to SSY vary with storm metric?
(3) Estimate annual SSY using the measurements from Objective 1, and modeling results from Objective 2. How does SSY at the field site compare to other volcanic tropical islands and other disturbed watersheds?

2. Study area

Faga'alu (Fong-uh ah-loo) watershed is located on Tutuila (14S, 170W), American Samoa, which is comprised of steep, heavily forested mountains with villages and roads mostly confined to the flat, coastal areas. The coral reef in Faga'alu Bay is highly degraded by sediment (Fenner et al., 2008) and Faga'alu watershed was selected by the US Coral Reef Task Force (USCRTF) as a Priority Watershed for conservation and remediation efforts (Holst-Rice et al., 2015).

The administrative boundary of Faga'alu includes the watersheds of the main stream (1.78 km^2) and several small ephemeral streams that drain directly to the bay (0.63 km^2) (grey dotted boundary in Fig. 1, "Admin."). Faga'alu watershed is drained by the main stream, which runs ~3 km from Matafao Mountain to Faga'alu Bay (area draining to FG3 in Fig. 1, "Total" watershed). The Total watershed can be divided into an undisturbed, Upper watershed (area draining to FG1, "Upper"), and a human-disturbed, Lower watershed (area draining to FG3, "Lower"). The Lower watershed can be further subdivided to isolate the impacts of an aggregate quarry (area draining between FG1 and FG2, "Lower_Quarry") and urbanized village area (area draining between FG2 and FG3, "Lower_Village") (Fig. 1).

Faga'alu occurs on intracaldera Pago Volcanics formed about 1.20 Mya (McDougall, 1985). Soil types in the steep uplands are rock outcrops (15% of the watershed area) and well-drained Lithic Hapludolls ranging from silty clay to clay loams 20–150 cm deep (Nakamura, 1984). Soils in the lowlands include a mix of deep (>150 cm), well drained very stony silty clay loams, and poorly drained silty clay to fine sandy loam along valley bottoms. The mean slope of Faga'alu watershed is 0.53 m/m and total relief is 653 m.

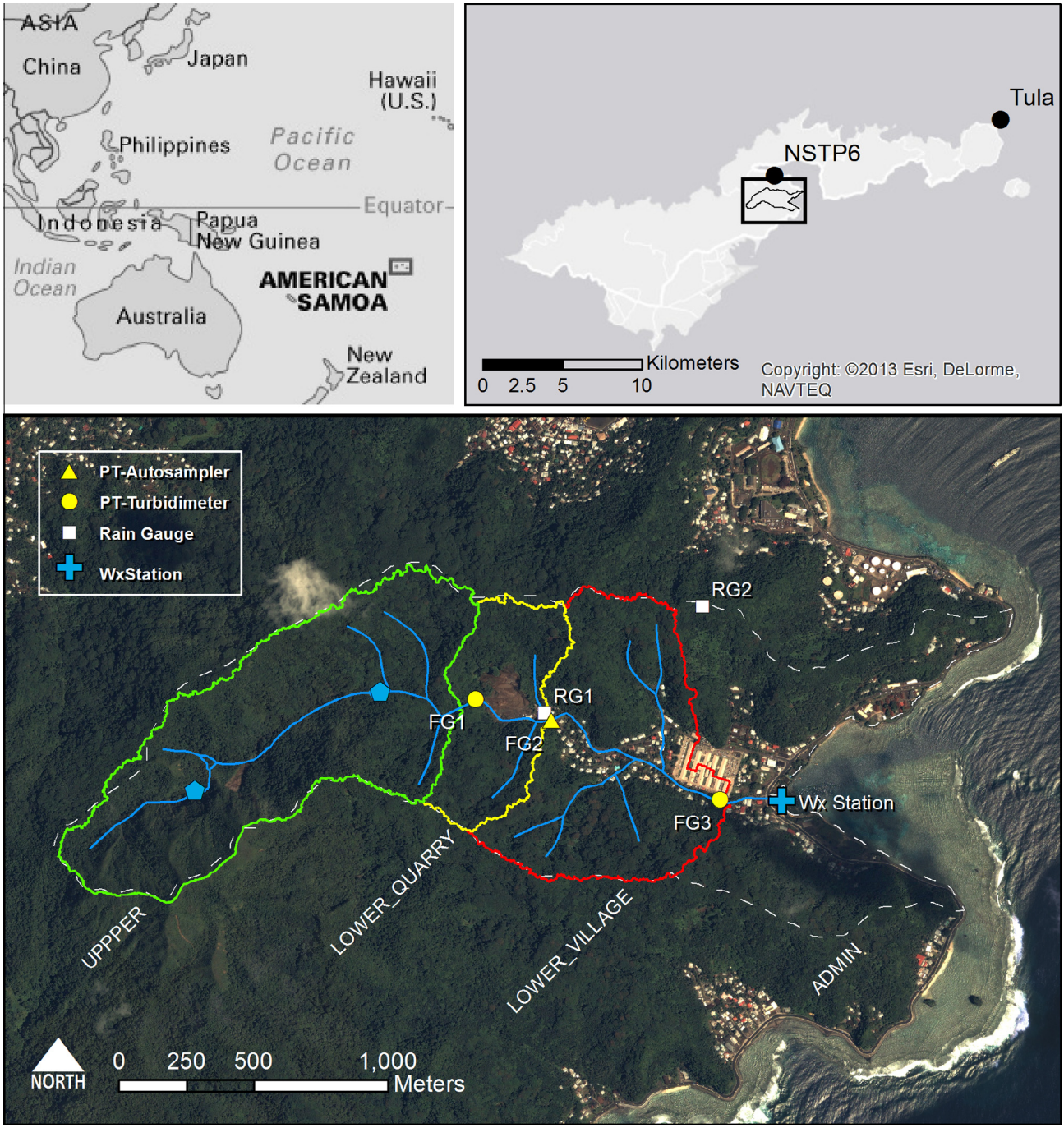

Fig. 1. Faga'alu watershed showing the Upper (undisturbed) and Lower (human-disturbed) subwatersheds. The Lower subwatershed drains areas between FG1 and FG3, and is further subdivided into the Lower_Quarry containing the quarry (between FG1 and FG2) and the Lower_Village containing the village areas (between FG2 and FG3). The Total watershed includes all subwatersheds draining to FG3. The Administrative watershed boundary for government jurisdiction is outlined by the dotted grey line. Blue pentagons in the Upper watershed show the location of abandoned water supply reservoirs (see Supplementary Material A for full description). Barometer locations at NSTP6 and TULA are shown in top-right. (For interpretation of the references to color in this figure legend, the reader is referred to the web version of this article.)

2.1. Climate

Annual precipitation in Faga'alu watershed is 6,350 mm at Matafao Mtn. (653 m m.a.s.l), 5,280 mm at Matafao Reservoir (249 m m.a.s.l.) and ~3,800 mm on the coastal plain (Craig, 2009; Dames and Moore, 1981; Perreault, 2010; Tonkin and Taylor International Ltd., 1989; Wong, 1996). There are two rainfall seasons: a drier winter from June through September accounts for 25% of annual *P*, and a wetter summer from October through May accounts for 75% of annual *P* (Craig, 2009; Perreault, 2010). *P* is lower in the drier season but large storms still occur: at 11 stream gages around the island, 35% of annual peak flows occurred during the drier season (1959–1990) (Wong, 1996).

2.2. Land cover and land use

2.2.1. Vegetation, agriculture, and urban areas

The predominant land cover in Faga'alu watershed is undisturbed vegetation on the steep hillsides (95%), including forest (86%) and scrub/shrub (9%) (Table 1). The Upper watershed is

Table 1
Land use categories in Faga'alu subwatersheds (NOAA Ocean Service and Coastal Services Center, 2010). Land cover percentages are of the subwatershed.

Subwatershed (outlet)	Cumulative area		Subwatershed area		Land cover as % subwatershed area[a]							
	km^2	%	km^2	%	B	HI	DOS	GA	F	S	Disturbed	Undisturbed
Upper (FG1)	0.9	50	0.90	50	0.4	0.0	0.0	0.1	82	17.1	0.4[b]	100
Lower_Quarry (FG2)	1.2	66	0.27	16	5.7	0.7	0.1	0.5	92	0.9	6.5	94
Lower_Village (FG3)	1.8	100	0.60	34	0.0	9.0	2.6	0.2	88	0.6	11.7	88
Lower (FG3)	1.8	100	0.88	50	1.8	6.4	1.8	0.3	89	0.7	10.1	90
Total (FG3)	1.8	100	1.78	100	1.1	3.2	0.9	0.2	86	9.0	5.2	95

[a] B = Bare, HI = High Intensity Developed, DOS = Developed Open Space, GA = Grassland (agriculture), F = Forest, S = Scrub/Shrub, Disturbed = B + HI + DOS + GA, Undisturbed = F + S.
[b] Disturbed area for Upper was from natural landslide. Undisturbed is 100% from rounding up.

dominated by undisturbed rainforest (82%) on steep hillslopes with no human disturbance. The Lower subwatershed has steep, vegetated hillslopes and a relatively small flat area in the valley bottom that is urbanized (6.4% "High Intensity Developed" in Table 1). A small portion of the watershed (1.8%) is developed open space, mainly landscaped lawns and parks. Agricultural areas include small household gardens and small areas of banana and taro on the steep hillsides, classified as grassland (0.3% GA, Table 1) due to high fractional grass cover. Most unpaved roads are stabilized with compacted gravel and do not appear to be a major sediment source (Horsley-Witten, 2012).

2.2.2. Aggregate quarry and reservoirs

An aggregate quarry covering 1.6 ha has been in continuous operation since the 1960s (Latinis et al., 1996) and accounted for nearly all of the bare land in Faga'alu watershed (1.1%) (Table 1). Sediment eroded from the quarry was discharged directly to Faga'alu stream until 2011, when quarry operators installed silt fences and small settling ponds (Horsley-Witten, 2011), which were inadequate to control the large amount of sediment mobilized during storms (Horsley-Witten, 2012). During the study period (2012–2014), additional sediment controls were installed and large piles of overburden were overgrown by vegetation (Fig. 2). In late 2014, after the monitoring reported here, large retention ponds were installed to capture sediment runoff. See Holst-Rice et al. (2015) for description of sediment mitigation at the quarry.

Three water impoundment structures were built in the early 1900s in the Upper watershed for drinking water supply and hydropower, but none are in use and the reservoir at FG1 is filled with coarse sediment. Other deep pools at the base of waterfalls in the upper watershed have no fine sediment and we assume the other reservoirs are not retaining fine suspended sediment. A full description of the reservoirs is in Supplementary Material A (Duvert and Gratiot, 2010; Kearns, 2013; URS Company, 1978).

3. Methods

The field methods used to calculate event-wise suspended sediment yield (SSY_{EV}) are described in Section 3.1. The equations and analytical methods used to accomplish Objectives 1–3 are described in Sections 3.2–3.4. Briefly, the in-stream suspended sediment yield (SSY, tons) and specific suspended sediment yield (sSSY, tons/km^2) (*sensu* Walling and Webb (1996)) were calculated for individual storm events (SSY_{EV}, $sSSY_{EV}$) at three locations in

Fig. 2. Photos of the aggregate quarry in Faga'alu in 2012, 2013, and 2014. Pictures a–b show vegetation overgrowth during the period of study from 2012 to 2014, and the location of the groundwater diversion that was installed in 2012. Pictures c–d show that haul roads were covered in gravel in 2013. Photos: Messina.

Faga'alu watershed using calculated discharge (Q) and suspended sediment concentration (SSC)(Fig. 1) (Section 3.1). Q was calculated from continuously recorded stage and a stage-discharge relationship calibrated with field measurements (Section 3.1.2). SSC was measured directly from grab samples or modeled from continuously monitored turbidity (T) and T–SSC relationships calibrated to in-stream SSC (Section 3.1.3). Storm events were identified using automated hydrograph separation, and SSY_{EV} calculated for each monitored location with the Q and SSC data (Section 3.2.1). The subwatersheds were nested, so SSY_{EV} contributions from subwatersheds were calculated by subtracting SSY_{EV} at the upstream subwatershed from SSY_{EV} at the given downstream subwatershed. SSY from disturbed surfaces was calculated assuming a spatially uniform SSY from forested parts of disturbed subwatersheds (Section 3.2.2). The cumulative probable error (PE) of SSY_{EV} was calculated for each storm to incorporate errors in Q and SSC, and different T–SSC relationships were tested for their impact on SSY estimates (Section 3.2.3). Log-linear regression models were developed to predict SSY_{EV} from storm metrics for the undisturbed and disturbed subwatersheds (Section 3.3). Annual SSY was estimated from the regression models and the ratio of annual storm precipitation to the precipitation during storms where SSY_{EV} was measured (Section 3.4).

Measurements of SSY at FG1, FG2 and FG3 quantify the in-stream suspended sediment budget. Other components of sediment budgets not measured in this study include channel erosion, channel deposition, and floodplain deposition (Walling and Collins, 2008). In Faga'alu, the channel bed is predominantly large volcanic cobbles and gravel, with no significant deposits of fine sediment. Upstream of the village, the valley is very narrow with no floodplain. In the Lower watershed the channel has been stabilized with cobble reinforced by fencing, so overbank flows and sediment deposition on the floodplain are not observed. We therefore assume that channel erosion and channel and floodplain deposition are insignificant components of the sediment budget, and the measured sediment yields at the three locations reflect differences in hillslope sediment supply.

3.1. Field data collection

Data on P, Q, SSC, and T were collected during four field campaigns: January–March 2012, February–July 2013, January–March 2014, and October–December 2014, and several intervening periods of unattended monitoring by instruments with data loggers. Field campaigns were scheduled to coincide with the period of most frequent storms in the November–May wet season, though large storms were sampled throughout the year.

3.1.1. Precipitation (P)

P was measured in Faga'alu watershed from January, 2012, to December, 2014, using a tipping-bucket rain gauge located at the quarry near the centroid of the watershed (RG1; 20 cm dia., 1-min resolution) and a Vantage Pro Weather Station located at the stream outlet to the ocean (Wx; 20 cm dia. 15-min resolution) (Fig. 1). Data from a third rain gauge, (RG2) was recorded from January to March, 2012 to determine an orographic precipitation relationship. Total event precipitation (P_{sum}) was calculated using 1 min interval data from RG1, with data gaps filled by 15-min interval precipitation data from Wx.

3.1.2. Water discharge (Q)

Stream gaging sites were chosen to take advantage of an existing control structure (FG1) and a stabilized stream cross section (FG3). At FG1 and FG3, Q was calculated from stream stage recorded at 15-min intervals using HOBO and Solinst pressure transducers (PT) and a stage-Q rating curve calibrated to Q measurements. Q was measured manually in the field over a range of flow conditions by the area-velocity method (AV) using a Marsh-McBirney flowmeter (Harrelson et al., 1994; Turnipseed and Sauer, 2010). Q measurements were not made at the highest stages recorded by the PTs, so the stage-Q rating curve at FG3 was extrapolated using Manning's equation, calibrating Manning's n (0.067) to the Q measurements. At FG1, the flow control structure is a masonry spillway crest, so the HEC-RAS model was used to create the stage-Q relationship and calibrated to Q measurements (Brunner, 2010). See Supplementary Material B for further details on stream gaging at FG1 and FG3.

A suitable site for stream gaging was not present at the outlet of the Lower_Quarry subwatershed (FG2), so water discharge at FG2 was calculated as the product of the specific water discharge from FG1 (m^3/km^2) and the watershed area draining to FG2 (1.17 km^2). The specific water discharge at FG2 is assumed to be the same as above FG1 since average slopes, vegetation, and soils of the watersheds are similar. Discharge may be higher from the quarry surface, which represents 5.7% of the Lower_Quarry subwatershed, so Q and SSY at FG2 are conservative, lower-bound estimates, particularly during small events when specific discharge from the Upper watershed was small relative to specific discharge from the quarry. The quarry surface is continually being disturbed, sometimes with large pits excavated and refilled in the course of weeks, as well as intentional water control structures implemented over time. Given the changes in the contributing area of the quarry, estimates of water yield from the quarry were uncertain, so we assumed a uniform specific discharge for the whole Lower_Quarry subwatershed.

3.1.3. Suspended sediment concentration (SSC)

SSC was estimated at 15 min intervals from either (1) linear interpolation of stream water samples, or (2) turbidity data (T) recorded at 15 min intervals and a T–SSC relationship calibrated to stream water samples. Stream water was collected by grab sampling with 500 mL HDPE bottles at FG1, FG2, and FG3. At FG2, water samples were also collected at 30 min intervals during storm events by an ISCO 3700 Autosampler triggered by a water level sensor. The Autosampler inlet tubing was oriented down-stream, just below the water level sensor, approximately 30 cm above the stream bed, on rebar positioned midstream. Samples were analyzed for SSC on-island using gravimetric methods (Gray, 2014; Gray et al., 2000). Water samples were vacuum filtered on pre-weighed 47 mm diameter, 0.7 μm Millipore AP40 glass fiber filters, oven dried at 100 °C for one hour, cooled and weighed to determine SSC (mg/L).

Interpolation of SSC from grab samples was performed if at least three samples were collected during a storm (Nearing et al., 2007), and if an SSC sample was collected within 30 min of peak Q. Based on low observed SSC between storm events, SSC was assumed to be zero at the beginning and end of each storm if no sample was available for those times (Lewis et al., 2001).

T was measured at FG1 and FG3 using three types of turbidimeters: (1) Greenspan TS3000 (TS), (2) YSI 600OMS with 6136 turbidity probe (YSI), and (3) two Campbell Scientific OBS500s (OBS). All turbidimeters were permanently installed in PVC housings near the streambed with the turbidity probe submerged at all flows and oriented downstream. Despite regular maintenance, debris fouling and vandalism caused frequent data loss.

Unique, linear T–SSC relationships were developed for the YSI and for each OBS turbidimeter at each location using linear regression on T data and SSC samples from storm periods (r^2 values 0.79–0.99, Supplementary Material C). The T–SSC relationship can be unique to each region, stream, instrument or even each storm event (Lewis et al., 2001), and can be influenced by water color, dissolved solids, organic matter, temperature, and particle shape,

size, and composition. Despite the multiple factors relating T to SSC, T is a robust predictor of SSC in streams (Gippel, 1995), and is most accurate when a unique T–SSC relationship is developed for each instrument and field site separately, using in situ SSC samples during storms (Lewis, 1996; Minella et al., 2008). The TS meter at FG1 was vandalized before sufficient samples had been collected to establish a T–SSC relationship for high T data, so the T–SSC relationship from the YSI was used for the TS data. Errors were higher at FG3 (RMSE 112% for YSI, 46% for OBS), and lower at FG1 (RMSE 13% for YSI at FG1). The T–SSC relationships for the YSI predicted higher SSC at FG3 than at FG1 for the same T value (Supplementary Material C), which introduces uncertainty in SSC and SSY at FG3. The impact of using the same T–SSC relationship at both FG1 and FG3 is tested in the error analysis (Section 3.2.3). The critical assumption in our application is that the parameters of the T–SSC relationship are stable over time and among storm events. The T–SSC relationships are critical to SSY calculations, so the cumulative error from these relationships were combined with other error sources to estimate uncertainty in SSY_{EV} (Section 3.2.3). See Supplementary Material C for further details on T–SSC relationships at FG1 and FG3.

3.2. SSY_{EV} for disturbed and undisturbed watersheds

3.2.1. Suspended Sediment Yield during storm events (SSY_{EV})

SSY_{EV} was calculated at FG1, FG2, and FG3 by integrating continuous Q and SSC (Duvert et al., 2012):

$$SSY_{EV} = k \int_{t=0}^{T} Q(t) * SSC(t) * dt \quad (1)$$

where SSY_{EV} is suspended sediment yield (tons) for an event from $t = 0$ at storm start to T = storm end, SSC is suspended sediment concentration (mg/L), Q is water discharge (L/s), and k converts from mg to tons (10^{-9}).

Storm events can be defined by P (Hicks, 1990) or Q data (Duvert et al., 2012), and the method used to identify storm events can significantly influence the analysis of SSY_{EV} (Gellis, 2013). Due to the large number of storm events and the prevalence of complex storm events observed at the study site, we used a digital filter signal processing technique (Nathan and McMahon, 1990) in the R-statistical package EcoHydRology (Fuka et al., 2014), which separates the hydrograph into quickflow, or direct surface or subsurface runoff that occurs during storms, and baseflow or delayed flow (Hewlett and Hibbert, 1967). Quickflow and baseflow components are not well defined in terms of hydrologic flow path; here we use the separation operationally to define storm events. Spurious events were sometimes identified due to instrument noise, so only events with quickflow lasting at least one hour and peak quickflow greater than 10% of baseflow were included (see Supplementary Material D for example).

The subwatersheds were nested (Fig. 1), so SSY_{EV} from subwatersheds was calculated as follows: SSY_{EV} from the Upper subwatershed, draining undisturbed forest, was sampled at FG1; SSY_{EV} from the Lower_Quarry subwatershed, draining undisturbed forest and the quarry between FG1 and FG2, was calculated as the difference between SSY_{EV} measured at FG1 and FG2; SSY_{EV} from the Lower_Village subwatershed, which drains undisturbed forest and the village between FG2 and FG3, was calculated as the difference between SSY_{EV} measured at FG2 and FG3; the Lower subwatershed, which drains undisturbed forest, the quarry, and village between FG1 and FG3, was calculated as the difference between SSY_{EV} measured at FG1 and FG3. SSY_{EV} from the Total watershed was measured at FG3 (Fig. 1; Table 1).

3.2.2. SSY from disturbed and undisturbed portions of subwatersheds

Land cover in the Lower subwatersheds (Lower_Quarry and Lower_Village) includes both undisturbed forest and human-disturbed surfaces (Table 1). SSY_{EV} from disturbed areas only was estimated as:

$$SSY_{EV\_distrb} = SSY_{EV\_subws} - (sSSY_{EV\_Upper} * Area_{undist}) \quad (2)$$

where SSY_{EV_distrb} is SSY_{EV} from disturbed areas only (tons), SSY_{EV_subws} is SSY_{EV} (tons) measured from the subwatershed, $sSSY_{EV\_Upper}$ is specific SSY_{EV} (tons/km^2) from the Upper subwatershed (SSY_{EV_FG1}), and $Area_{undist}$ is the area of undisturbed forest in the subwatershed (km^2). This calculation assumes that forests in all subwatersheds have SSY similar to the Upper watershed.

The disturbance ratio (DR) is the ratio of SSY_{EV} under current conditions to SSY_{EV} under pre-disturbance conditions:

$$DR = \frac{SSY_{EV\_subw}}{A_{subw} * sSSY_{EV\_Upper}} \quad (3)$$

where A_{subw} is the area of the subwatershed. Both Eqs. (2) and (3) assume that $sSSY_{EV}$ from forested areas in the Lower subwatershed equals $sSSY_{EV}$ from the undisturbed Upper watershed and that pre-disturbance land cover was forested throughout the watershed.

3.2.3. Error analysis

Uncertainty in SSY_{EV} calculations arises from errors in measured and modeled Q and SSC (Harmel et al., 2006). The root mean square error propagation method estimates the "most probable value" of the cumulative or combined error by propagating the error from each measurement and modeling procedure, i.e. stage-Q and T–SSC, to the final SSY_{EV} calculation (Topping, 1972). The resulting cumulative probable error (PE) is the square root of the sum of the squares of the maximum values of the separate errors:

$$PE = \sqrt{\left(E_{Qmeas}^2 + E_{SSCmeas}^2\right) + \left(E_{Qmod}^2 + E_{SSCmod}^2\right)} \quad (4)$$

where PE is the cumulative probable error for SSY_{EV} estimates (±%), E_{Qmeas} is uncertainty in Q measurements (±%), $E_{SSCmeas}$ is uncertainty in SSC measurements (±%), E_{Qmod} is uncertainty in the Stage-Q relationship (RMSE, as ±% of the mean observed Q), E_{SSCmod} is uncertainty in the T–SSC relationship or from interpolating SSC samples (RMSE, as ±% of the mean observed SSC) (Harmel et al., 2009). E_{Qmeas} and $E_{SSCmeas}$ were taken from the DUET-H/WQ software tool lookup tables (Harmel et al., 2009).

The effect of uncertain SSY_{EV} estimates may complicate conclusions about anthropogenic impacts and storm metric-SSY_{EV} relationships, but differences in SSY_{EV} from undisturbed and disturbed areas were expected to be much larger than the cumulative uncertainty. High uncertainty is common in sediment yield studies where successful models estimate SSY with ±50–100% accuracy (Calhoun and Fletcher, 1999; Duvert et al., 2012). PE was calculated for SSY_{EV} from the Upper and Total watersheds, but not for the Lower subwatershed since it was calculated as the difference of SSY_{EV_UPPER} and SSY_{EV_TOTAL}.

In addition to the error due to scatter about a given T–SSC relationship, there may also be uncertainty about the regression line itself, particularly where a given instrument shows different T–SSC relationships at different locations (Supplementary Material C). In Faga'alu, the T–SSC relationships estimated higher SSC for a given T value at the disturbed site (FG3) than at the forested site (FG1). In order to test for the impact of using the same T–SSC relationship at both locations, we recalculated SSY_{EV} and the disturbance ratio using the T–SSC relationship at FG3 to estimate SSC at both FG3 and FG1.

3.3. Modeling SSY_{EV} with storm metrics

The relationship between SSY_{EV} and storm metrics was modeled as a log-linear function:

$$SSY_{EV} = \alpha X^{\beta} * BCF \quad (5)$$

where X is a storm metric, the regression coefficients α and β are obtained by ordinary least squares regression on the logarithms of X and SSY_{EV} (Basher et al., 2011; Duvert et al., 2012; Hicks, 1990) and BCF is the Smearing bias correction factor for log-transformation bias (Duan, 2016; USGS and NRTWQ, 2016), which is recommended when residuals of the log–log regression are non-normal (Boning, 1992; Koch and Smillie, 1986). The Kolmogorov–Smirnov test showed the regression residuals were non-normally distributed.

Four storm metrics were tested as predictors of SSY_{EV}: Total event precipitation (P_{sum}), event Erosivity Index (EI) (Hicks, 1990; Kinnell, 2013), total event water discharge (Q_{sum}), and maximum event water discharge (Q_{max}) (Duvert et al., 2012; Rodrigues et al., 2013). The Erosivity Index describes the erosive power of rainfall and was calculated for each storm event identified in Section 3.2.1 following the methodology of Kinnell (2013) using only 1 min interval data at RG1. The discharge metrics (Q_{sum} and Q_{max}) were normalized by watershed area to compare different sized subwatersheds.

Model fits for each storm metric were compared using coefficients of determination (r^2) and Root Mean Square Error (RMSE). The correlation between storm metrics (X) and SSY_{EV} were quantified using non-parametric (Spearman) correlation coefficients. The regression coefficients (α and β) for the Upper and Total watersheds were tested for statistically significant differences using Analysis of Covariance (ANCOVA) (Lewis et al., 2001).

3.4. Estimation of annual SSY

Annual SSY (mass) and sSSY (mass/area) were estimated using (1) the developed storm metric-SSY_{EV} models, and (2) the ratio of annual storm precipitation to precipitation measured during storms with SSY_{EV} data.

An annual SSY time-series was not possible due to the discontinuous field campaigns and failure of or damage to the turbidimeters. Continuous records of P and Q were available for 2014, so the log-linear storm metric-SSY_{EV} models (Eq. (5)), including log-bias correction (Duan, 2016; Ferguson, 1986), were used to predict SSY_{EV} for all storms in 2014 (Basher et al., 1997). For storms missing Q_{max} data at FG3, Q_{max} was predicted from a linear regression between Q_{max} at FG1 and Q_{max} at FG3 for the study period ($R^2 = 0.88$).

Annual SSY and sSSY were also estimated by multiplying SSY_{EV} from measured storms by the ratio of annual storm precipitation (P_{EVann}) to precipitation during storms where SSY_{EV} was measured (P_{EVmeas}):

$$SSY_{ann} = SSY_{EV\_meas} * \frac{P_{EVann}}{P_{EVmeas}} \quad (6)$$

where SSY_{ann} is estimated annual SSY during storms, SSY_{EV_meas} is SSY_{EV} from sampled storms (all, Tables 2 and 4), P_{EVann} is the precipitation during all storm events in a year, where storms are defined using hydrograph separation (3.2.1), and P_{EVmeas} is precipitation during the set of sampled storms. Eq. (6) assumes that the sediment yield per mm of storm precipitation is constant over the year, and insensitive to the size distribution of storms, though there is evidence that SSY_{EV} increases exponentially with storm size (Lewis et al., 2001; Rankl, 2004). Eq. (6) also ignores sediment yield during non-storm periods, which is justified by the low SSC (typically under 20 mg/L) and Q (baseflow) observed between storms.

4. Results

4.1. Field data collection

4.1.1. Precipitation

At RG1, P was 3,502 mm, 3,529 mm, and 3,709 mm in 2012, 2013, and 2014, respectively, which averages 94% of long-term P (=3,800 mm) (PRISM data; Craig, 2009). Daily P at RG1 was similar to P at Wx (regression slope = 0.95, $r^2 = 0.87$) and at RG2 (slope = 0.75, $r^2 = 0.85$). Higher P was expected at higher elevation at RG2 so lower P at RG2 was assumed to be caused by measurement error, as the only available sampling location was a forest clearing with high surrounding canopy. P measured at higher elevations would be useful to determine the orographic effect, but for this analysis the absolute values of P in each subwatershed are not as important since P and the Erosivity Index are only used as predictive storm metrics. Given the near 1:1 relationship between daily P measured at RG1 and Wx, P was assumed to be homogenous over the Lower subwatershed.

4.1.2. Water discharge (Q)

Q at FG1 and FG3 was characterized by low but perennial baseflow, punctuated by flashy hydrograph peaks (Fig. 3). Storm events were generally smaller but more frequent in the October–April wet season compared to the May–September dry season, when the largest event in the three year monitoring period was observed (August 2014).

4.1.3. Suspended Sediment Concentrations (SSC) during storm and non-storm periods

An example of a storm event on 2/14/2014 (Fig. 4) shows that SSC at FG2 was highest on the rising limb of the hydrograph, and that T and SSC at FG3 were always higher than at FG1. SSC was consistently lowest at FG1, highest downstream of the quarry (FG2), and intermediate downstream of the village (FG3), during both storm and non-storm periods (Fig. 5a and b). Mean and maximum SSC of all stream water samples were lowest at FG1 ($\mu = 28$ mg/L, max = 500 mg/L, $n = 59$), highest at FG2 ($\mu = 337$ mg/L, max = 12,600 mg/L, $n = 90$), and intermediate at FG3 ($\mu = 148$ mg/L, max = 3500 mg/L, $n = 159$). SSC data at FG1-3 were non-normal, so non-parametric significance tests were applied. SSC was significantly different among the three sites during non-storms and storms ($p < 10^{-4}$). Pair-wise Mann–Whitney tests between FG1 and FG2 were significant ($p < 10^{-4}$ for both storms and non-storms). FG2 and FG3 were significantly different for non-storm periods ($p < 0.05$) but not for storms ($p > 0.10$) due to the high variance.

SSC varied by several orders of magnitude for a given Q at FG1-3 (Fig. 6) due to significant hysteresis observed during storm periods (Fig. 4). Maximum SSC at FG1 (500 mg/L) was sampled on 04/23/2013 at high Q ($Q_{FG1} = 3724$ L/s) (Fig. 6a). Maximum SSC at FG2 (12,600 mg/L) and FG3 (3500 mg/L) were sampled during the same storm (03/05/2012) when brief but intense P caused high SSC runoff from the quarry, but Q was low (Fig. 6b and c). SSC was diluted downstream of the quarry by the addition of runoff with lower SSC from the village and forest draining to FG3.

4.2. SSY_{EV} for disturbed and undisturbed watersheds

A total of 210 storms were identified January, 2012, to December, 2014. A total of 169 storms had Q data at both FG1 and FG3

(Supplementary Material D, Table 1). SSC data were recorded during 112 (FG1) and 74 storms (FG3). Of those storms, 42 had *P*, *Q*, and SSC data at FG1 and FG3. Of those storms, 8 had *P*, *Q*, and SSC data at FG2. Storm events ranged from 1 h to 2 days, with mean duration of 13 h.

4.2.1. Suspended sediment yield during storm events (SSY_{EV}) from Upper, Lower, and Total watersheds

For the 42 storms with *P*, *Q*, and SSC data at both FG1 and FG3, SSY_{EV_Total} was 129 ± 121 tons, with 17 ± 7 tons from the Upper watershed and 112 tons from the Lower subwatershed (Table 2). The Upper and Lower subwatersheds are similar in size (0.90 km^2 and 0.88 km^2) but SSY_{EV_Lower} accounted for 87% of SSY_{EV} at the watershed outlet. The DR (Eq. (4), $sSSY_{EV}$_Upper = 18.8 tons/km^2) suggests $sSSY_{EV}$ has increased by 6.8× in the Lower subwatershed, and 3.9× for the Total watershed compared with undisturbed forest in the Upper watershed.

4.2.2. SSY from disturbed and undisturbed portions of Upper, Lower, and Total watersheds

In the Lower subwatershed, disturbed areas cover 10% of the surface but contributed 87% of SSY_{EV_Lower}. In the Total watershed, disturbed areas cover only 5.2% of the surface but contributed 75% of SSY_{EV_Total}. sSSY from disturbed areas in the Lower subwatershed was 1095 tons/km^2, or 58× the sSSY of undisturbed forest (Table 3).

4.2.3. Suspended sediment yield during storm events (SSY_{EV}) from Lower_Quarry and Lower_Village watersheds

For the 8 storms with *P*, *Q*, and SSC data at FG1-3, sSSY from the Upper, Lower_Quarry, Lower_Village, and the Total watershed was 15, 61, 27, and 26 tons/km^2, respectively, with 29% of SSY_{EV} from the Upper subwatershed, 36% from the Lower_Quarry subwatershed, and 35% from the Lower_Village subwatershed. The storms in Table 4 may underrepresent the contributions of the quarry

Table 2
Event-wise suspended sediment yield (SSY_{EV}) from subwatersheds in Faga'alu for events with simultaneous data from FG1 and FG3. Storm numbers correspond with the storms presented in Supplementary Material D Table 1.

Storm#	Storm	Precip	SSY_{EV} tons			% of SSY_{EV_Total}		PE[a]		SSC	
	Start	mm	Upper[b]	Lower[c]	Total[d]	Upper	Lower	Upper	Total	Data source upper	Data source total
2	01/19/2012	18	0.06	0.63	0.69	8.0	91.0	56	36	T-TS	int. grab
4	01/31/2012	35	0.03	1.92	1.95	1.0	98.0	56	118	T-TS	T-YSI
5	02/01/2012	11	0.01	0.4	0.42	3.0	96.0	56	118	T-TS	T-YSI
6	02/02/2012	16	0.06	1.02	1.08	5.0	94.0	56	118	T-TS	T-YSI
7	02/03/2012	11	0.08	2.01	2.09	3.0	96.0	56	118	T-TS	T-YSI
8	02/04/2012	6	0.0	0.51	0.51	0.0	99.0	56	118	T-TS	T-YSI
9	02/05/2012	23	0.05	0.98	1.03	5.0	94.0	56	118	T-TS	T-YSI
10	02/05/2012	21	0.09	1.93	2.02	4.0	95.0	56	118	T-TS	T-YSI
11	02/06/2012	38	0.28	4.75	5.03	5.0	94.0	56	118	T-TS	T-YSI
12	02/07/2012	4	0.01	0.13	0.15	9.0	90.0	56	118	T-TS	T-YSI
13	02/07/2012	10	0.03	0.51	0.54	5.0	94.0	56	118	T-TS	T-YSI
14	02/13/2012	11	0.0	0.27	0.27	1.0	98.0	56	118	T-TS	T-YSI
16	03/05/2012	22	0.0	4.39	4.4	0.0	99.0	56	118	T-TS	T-YSI
17	03/06/2012	56	0.19	9.05	9.25	2.0	97.0	56	118	T-TS	T-YSI
18	03/08/2012	22	0.09	2.89	2.98	2.0	97.0	56	118	T-TS	T-YSI
19	03/09/2012	19	0.2	2.78	2.97	6.0	93.0	56	118	T-TS	T-YSI
20	03/15/2012	17	0.01	1.17	1.18	0.0	99.0	56	118	T-TS	T-YSI
21	03/16/2012	34	0.08	2.12	2.2	3.0	96.0	56	118	T-TS	T-YSI
22	03/17/2012	32	0.09	3.33	3.43	2.0	97.0	56	118	T-TS	T-YSI
23	03/20/2012	24	0.04	0.84	0.88	4.0	95.0	56	118	T-TS	T-YSI
24	03/21/2012	18	0.2	2.06	2.26	8.0	91.0	56	118	T-TS	T-YSI
25	03/22/2012	34	0.37	5.75	6.12	5.0	94.0	56	118	T-TS	T-YSI
27	03/24/2012	7	0.03	0.19	0.22	12.0	87.0	56	118	T-TS	T-YSI
28	03/25/2012	49	0.7	11.92	12.62	5.0	94.0	56	118	T-TS	T-YSI
29	03/31/2012	15	0.03	0.78	0.81	3.0	96.0	56	118	T-TS	T-YSI
32	05/07/2012	11	0.0	1.31	1.31	0.0	99.0	56	118	T-TS	T-YSI
33	05/08/2012	21	0.13	6.65	6.79	1.0	98.0	56	118	T-TS	T-YSI
34	05/20/2012	13	0.0	0.47	0.48	0.0	99.0	56	118	T-TS	T-YSI
64	04/16/2013	62	0.54	4.01	4.55	11.0	88.0	40	36	int. grab	int. grab
70	04/23/2013	86	9.57	13.51	23.08	41.0	58.0	40	36	int. grab	int. grab
79	06/24/2013	9	0.01	0.13	0.14	7.0	92.0	43	77	T-YSI	T-OBS
80	07/02/2013	13	0.02	0.28	0.3	5.0	94.0	43	77	T-YSI	T-OBS
106	02/14/2014	25	0.26	1.57	1.82	14.0	85.0	43	51	T-YSI	T-OBS
107	02/15/2014	7	0.04	0.63	0.67	6.0	93.0	43	51	T-YSI	T-OBS
109	02/18/2014	12	0.01	0.81	0.81	0.0	99.0	43	51	T-YSI	T-OBS
110	02/20/2014	29	0.13	3.71	3.84	3.0	96.0	43	51	T-YSI	T-OBS
111	02/21/2014	51	2.55	7.03	9.58	26.0	73.0	43	51	T-YSI	T-OBS
112	02/24/2014	16	0.09	0.56	0.65	13.0	86.0	43	51	T-YSI	T-OBS
113	02/24/2014	1	0.01	0.12	0.13	9.0	90.0	43	51	T-YSI	T-OBS
114	02/25/2014	67	0.62	7.17	7.79	7.0	92.0	43	51	T-YSI	T-OBS
115	02/27/2014	16	0.13	0.68	0.8	15.0	84.0	43	51	T-YSI	T-OBS
116	02/27/2014	12	0.12	1.25	1.37	8.0	91.0	43	51	T-YSI	T-OBS
Total/Avg	42	1004	17.0	112.2	129.2	13	87	52	94	–	–
Tons/km^2	–	–	18.8	127.5	72.6	–	–	–	–	–	–
DR	–	–	1	6.8	3.9	–	–	–	–	–	–

[a] PE is cumulative probable error (Eq. (4)) as a percentage of the mean observed SSY_{EV}.
[b] Measured SSY_{EV} at FG1.
[c] SSY_{EV} at FG3 – SSY_{EV} at FG1.
[d] Measured SSY_{EV} at FG3.

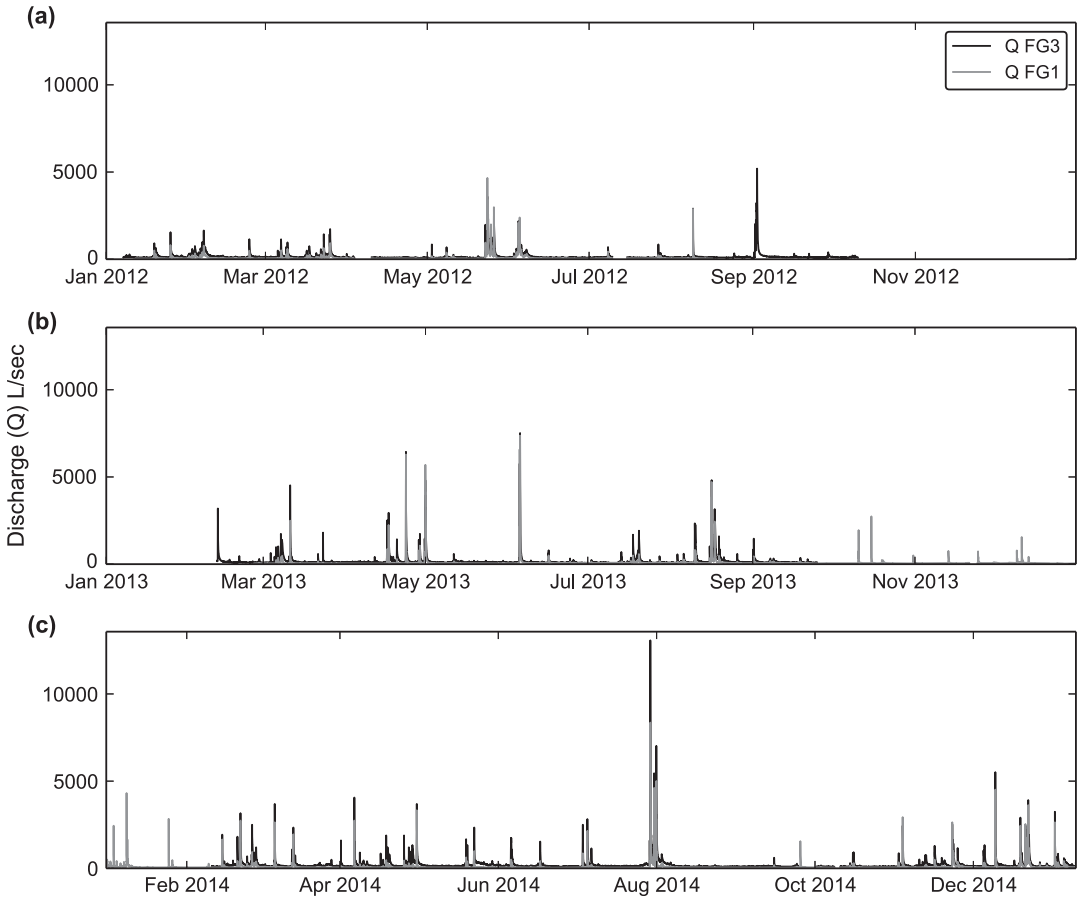

Fig. 3. Time series of water discharge (Q) at FG1 and FG3, calculated from measured stage and the stage-discharge rating curves in (a) 2012, (b) 2013 and (c) 2014.

and village to SSY, since they show a lower DR for the Total watershed (1.7× SSY_{Upper}) compared with the 42 storms in Table 2 (3.9× SSY_{Upper}). sSSY increased by 4.1× in the Lower_Quarry subwatershed and 1.8× in the Lower_Village subwatershed compared with the undisturbed Upper watershed.

4.2.4. SSY from disturbed and undisturbed portions of Lower_Quarry and Lower_Village watersheds

Disturbed areas cover small fractions of the subwatersheds, yet contributed roughly 77% of $SSY_{EV\_Lower\_Quarry}$ (6.5% disturbed) and 51% of $SSY_{EV\_Lower\_Village}$ (11.7% disturbed). Similarly, disturbed areas cover 5.2% of the Total watershed but contributed 75–45% of SSY_{EV_Total} (Tables 3 and 5). sSSY from disturbed areas in the Upper (37 tons/km^2), Lower_Quarry (722 tons/km^2), and Lower_Village subwatersheds (116 tons/km^2) suggested that disturbed areas increase sSSY over forested conditions by 49× and 8× in the Lower_Quarry and Lower_Village subwatersheds, respectively. Human disturbance in the Lower_Village subwatershed increased SSY_{EV} above natural levels but the magnitude of disturbance was much lower than the quarry.

4.2.5. Error analysis

Cumulative Probable Errors (PE) in SSY_{EV}, calculated from measurement and model errors in Q and SSC data, were 40–56% (μ = 52%) at FG1 and 36–118% (μ = 94%) at FG3.

The measurement error for Q at FG1 and FG3 was 8%, including area-velocity measurements (6%), continuous Q measurement in a natural channel (6%), pressure transducer error (0.1%), and streambed condition (firm, stable bed = 0%) (DUET-H/WQ look-up table (Harmel et al., 2006)). Model errors were 32% for the stage-Q rating curve using Manning's equation at FG3, and 22% using HEC-RAS at FG1 (Supplementary Material B).

The measurement error for SSC was 16%, including interpolating over a 30 min interval (5%), sampling during stormflows (3%), and measuring SSC by filtration (3.9%) (DUET-H/WQ look-up table (Harmel et al., 2006)). Model errors of the *T*–SSC relationships were 13% (3 mg/L) for the YSI and TS turbidimeters at FG1, 112% (342 mg/L) for the YSI turbidimeter at FG3, and 47% (46 mg/L) for the OBS turbidimeter at FG3 (Supplementary Material C).

SSC and resulting SSY_{EV} estimates are sensitive to the slope of the *T*–SSC rating curve, so we tested the sensitivity of the DR and percent SSY contributions to different *T*–SSC rating curves. The slope of the *T*–SSC rating curve for the YSI, deployed at FG3 in 2012, was higher at FG3 than at FG1 (Supplementary Material C, Fig. C.1a and b). Using the *T*–SSC relationship from FG1 to predict SSC at FG3 reduced the DR from 3.6 (Table 2) to 2.5, and changed the average SSY_{EV} contributions from 13% to 20% from the Upper watershed, and from 87% to 80% from the Total watershed. We conclude that use of different *T*–SSC relationships does not significantly change our conclusions about the dominance of the Lower watershed in the sediment load to the coast.

4.3. Modeling SSY_{EV} with storm metrics

4.3.1. Selecting the best predictor of SSY_{EV}

Q_{sum} and Q_{max} were the best predictors of SSY_{EV} for the forested Upper watershed, and Q_{max} was the best predictors for the Total watershed (Fig. 7, Table 6). SSY_{EV} is calculated from Q so it is expected that Q_{sum} correlated closely with SSY_{EV} (Duvert et al., 2012; Rankl, 2004). Discharge metrics were highly correlated with

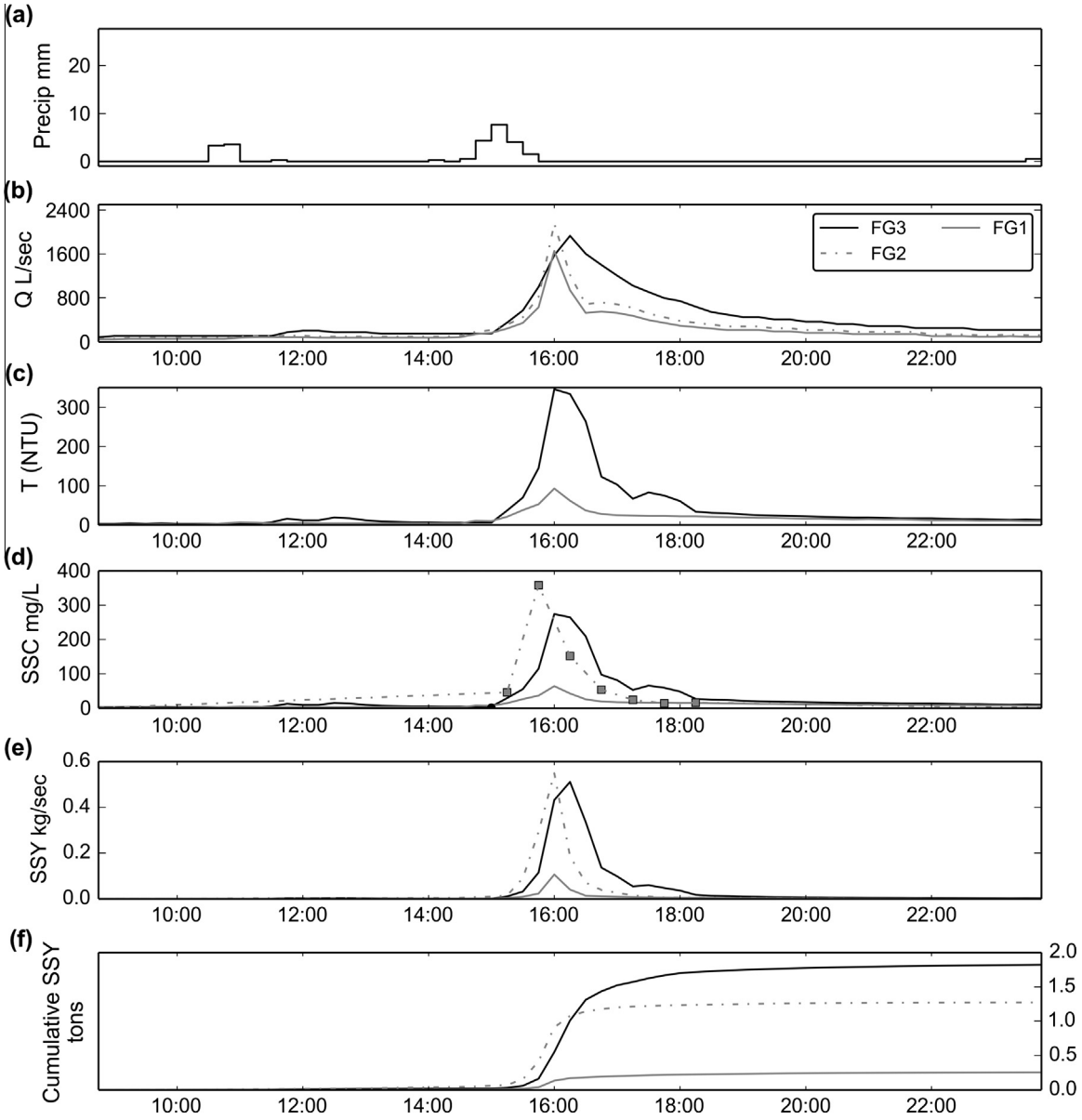

Fig. 4. Example of a storm event (02/14/2014). SSY at FG1 and FG3 calculated from SSC modeled from *T*, and SSY at FG2 from SSC samples collected by the Autosampler.

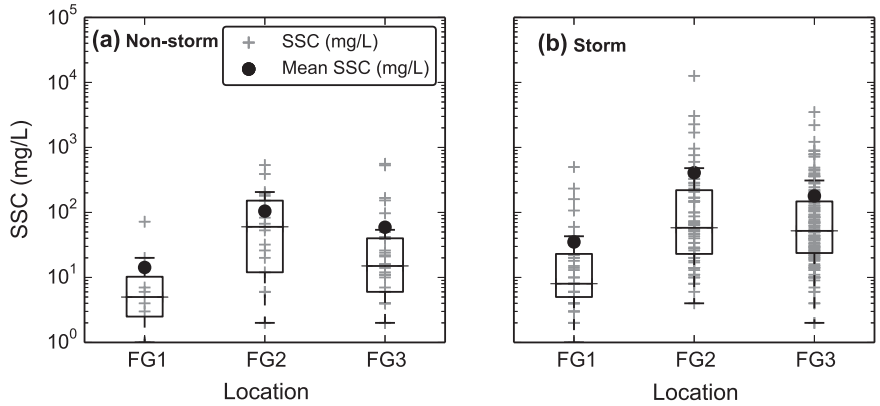

Fig. 5. Boxplots of Suspended Sediment Concentration (SSC) from grab samples only (no Autosampler) at FG1, FG2, and FG3 during (a) non-stormflow and (b) stormflow.

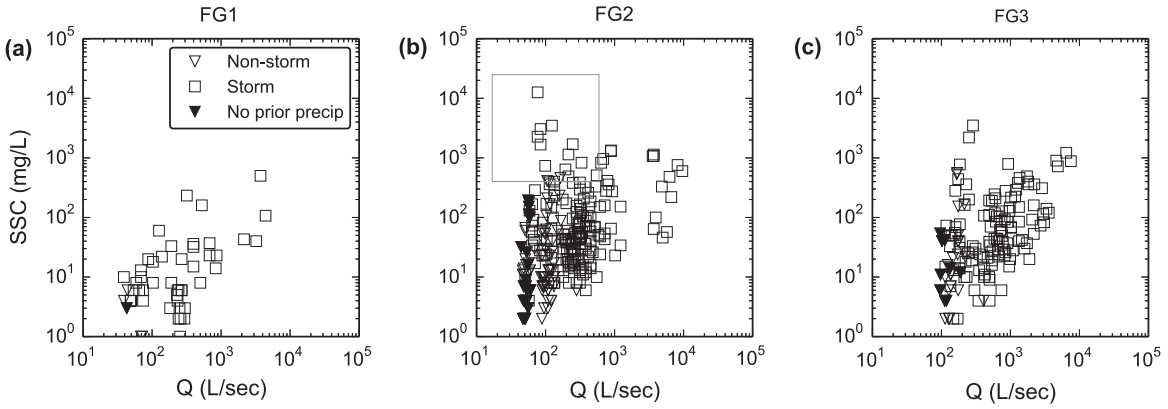

Fig. 6. Water discharge (*Q*) versus suspended sediment concentration (SSC) measured from stream water samples at (a) FG1, (b) FG2, and (c) FG3 during non-stormflow and stormflow periods. The box in (b) highlights the samples with high SSC during low flows. Solid symbols indicate SSC samples where precipitation during the preceding 24 h was 0 mm.

Table 3
Suspended sediment yield (SSY), specific suspended sediment yield (sSSY), and disturbance ratio (DR) from disturbed portions of Upper and Lower subwatersheds for the storm events in Table 2.

	Upper[a]	Lower	Total
Fraction of subwatershed area disturbed (%)	0.4	10.1	5.2
SSY (tons)	17.0	112.2	129.2
Forested areas	16.9	14.9	31.7
Disturbed areas	0.1	97.3	97.5
% from disturbed areas	0.9	87	75
sSSY, disturbed areas (tons/km^2)	41.0	1095.0	1053.1
DR for sSSY from disturbed areas[b]	2	58	56

[a] Disturbed areas in Upper are bare areas from landslides.
[b] Calculated as (sSSY from disturbed areas)/sSSY from Upper (17.0 tons/km^2)

SSY_{EV} in the Total watershed, suggesting they are good predictors in both disturbed and undisturbed watersheds. Most of the scatter in the Q_{max}–SSY_{EV} relationship is observed for small events, and Q_{max} correlated strongly with the largest SSY_{EV} values, when most of the annual SSY is generated (Fig. 7a).

4.3.2. Effect of event size and watershed disturbance

In general, SSY_{EV_Total} was higher than SSY_{EV_Upper} for the full range of measured storms with the exception of a few events. The outlier events could be from measurement error or mass movements in the Upper watershed. The event with much higher SSY_{EV} at FG1 (Fig. 7d) did not have corresponding data for FG2 or FG3, to determine if this event was data error. The separation of multi-peak storm events, storm sequence, and antecedent conditions may also play a role. While strong seasonality is not observed in Faga'alu, low rainfall can persist for several weeks, perhaps altering water and sediment dynamics in subsequent storm events.

A higher intercept (α) for the human-disturbed compared to the undisturbed watershed indicates higher SSY_{EV} for the same size storm event. A difference in slope (β) indicates the relative subwatershed contributions vary with storm size. All storm metric-SSY_{EV} model intercepts (α) were significantly different ($p < 0.01$), but only the Q_{sum}–SSY_{EV} model showed significantly different slopes (β, $p < 0.01$) (Fig. 7, Table 6). The relative sediment contribution from the human-disturbed watershed was hypothesized to diminish with increasing storm size, but the results from *P* and *Q* metrics were contradictory. The Q_{sum}–SSY_{EV} model indicates a decrease in relative contribution from the disturbed Lower watershed, but the P_{sum}– and Q_{max}–SSY_{EV} models show no change over increasing storm size (Fig. 7). It was hypothesized that SSY_{EV} from undisturbed forest would become the dominant source for larger storms, but the DR remains high for large storms due to naturally low SSY_{EV} from forest areas in Faga'alu watershed. This suggests that disturbed areas were not supply limited for the range of sampled storms.

Table 4
Event-wise suspended sediment yield (SSY_{EV}) from subwatersheds in Faga'alu for events with simultaneous data from FG1, FG2, and FG3. Storm numbers correspond with the storms presented in Table 2 and Supplementary Material D Table 1.

Storm#	Storm	Precip	SSY_{EV} tons					% of SSY_{EV_TOTAL}			
	Start	mm	Upper[a]	Lower_Quarry[b]	Lower_Village[c]	Lower[d]	Total[e]	Upper	Lower_Quarry	Lower_Village	Lower
2	01/19/2012	18	0.06	0.30	0.33	0.63	0.69	8.0	43	47	91
64	04/16/2013	62	0.54	2.77	1.24	4.01	4.55	11.0	60	27	88
70	04/23/2013	86	9.57	8.21	5.30	13.51	23.08	41.0	35	22	58
106	02/14/2014	25	0.26	1.01	0.55	1.57	1.82	14.0	55	30	86
110	02/20/2014	29	0.13	1.60	2.11	3.71	3.84	3.0	41	54	96
111	02/21/2014	51	2.55	2.07	4.96	7.03	9.58	26.0	21	51	73
115	02/27/2014	16	0.13	0.08	0.59	0.68	0.80	16.0	9	73	85
116	02/27/2014	12	0.12	0.32	0.93	1.25	1.37	8.0	23	67	91
Total/Avg	8	299	13.4	16.4	16.0	32.4	45.7	29	36	35	71
Tons/km^2			14.8	60.6	26.7	36.8	25.7	–	–	–	–
DR			1.0	4.1	1.8	2.5	1.7	–	–	–	–

[a] Measured SSY_{EV} at FG1.
[b] SSY_{EV} at FG2 – SSY_{EV} at FG1.
[c] SSY_{EV} at FG3 – SSY_{EV} at FG2.
[d] SSY_{EV} at FG3 – SSY_{EV} at FG1.
[e] Measured SSY_{EV} at FG3.

Table 5
Suspended sediment yield (SSY), specific suspended sediment yield (sSSY), and disturbance ratio (DR) from disturbed portions of Upper, Lower_Quarry, and Lower_Village subwatersheds for the storm events in Table 4.

	Upper	Lower_Quarry	Lower_Village	Lower	Total
Fraction of subwatershed area disturbed (%)	0.4	6.5	11.7	10.1	5.2
SSY (tons)	13.4	16.4	16.0	32.4	45.7
Forested areas	13.3	3.7	7.8	11.7	25.0
Disturbed areas	0.1	12.7	8.2	20.7	20.7
% from disturbed areas	1	77	51	64	45
sSSY, disturbed areas (tons/km^2)	37.0	721.6	116.2	232.8	223.9
DR for sSSY from disturbed areas	3	49	8	16	15

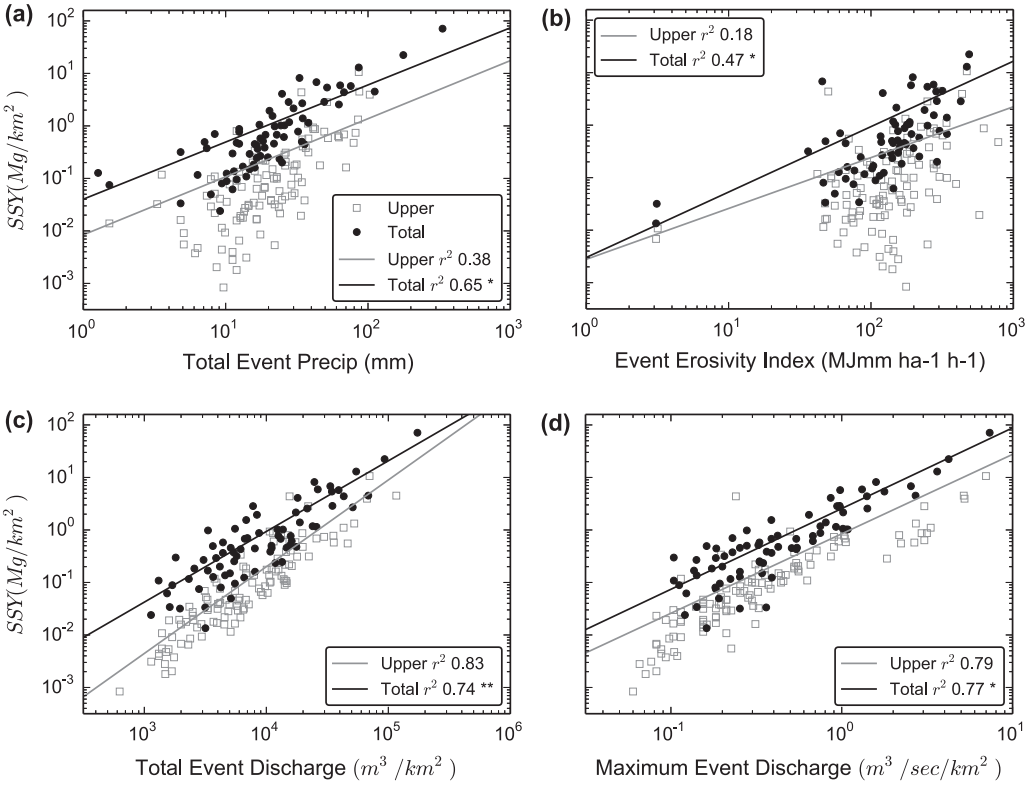

Fig. 7. sSSY$_{EV}$ regression models for storm metrics. Each point represents a different storm event. ** = slopes and intercepts were statistically different ($p < 0.01$), * = intercepts were statistically different ($p < 0.01$).

4.4. Estimation of annual SSY

Annual SSY estimates varied, depending on which storm metric or set of storms (all, Tables 2 and 4) was used. The Q_{max} models (with bias correction) and Eq. (6) using all events gave different annual SSY estimates at both the Upper watershed (41–129 tons/yr) and the Total watershed (655–428 tons/yr). The P_{sum} model resulted in much lower estimates due to higher scatter about the P_{sum}-SSY$_{EV}$ relationship for large events, even with bias correction, compared with the more robust Q_{max}–SSY$_{EV}$ model (Table 7). The Q_{max}–SSY$_{EV}$ model prediction is sensitive to the storm-size distribution, with significantly more SSY$_{EV}$ for events with higher Q_{max}. Comparing annual SSY estimates from different methods, using different sets of storm sizes can therefore make it appear that there is much disagreement when in fact this variability arises mostly from the variation in storm size distribution.

Annual storm precipitation (P_{EVann}) in 2014 was 2,770 mm, representing 69% of total annual precipitation (3,709 mm). The remaining 31% of precipitation did not result in a rise in stream level sufficient to be classified as an event with the hydrograph separation method. All storms with measured SSY$_{EV_Upper}$ from 2012 to 2014 included 3,457 mm of precipitation (P_{EVmeas}), or 125% of P_{EVann}, so estimated annual SSY$_{Upper}$ (Eq. (6)) was 41 tons/yr (45 tons/km^2/yr). All storms with measured SSY$_{EV_Total}$ from 2012 to 2014 included 2.628 mm of precipitation, or 95% of expected annual storm precipitation so estimated annual SSY$_{Total}$ was 428 tons/yr (241 tons/km^2/yr).

5. Discussion

5.1. SSC and SSY$_{EV}$ for disturbed and undisturbed watersheds

5.1.1. SSC for disturbed and undisturbed watersheds in Faga'alu

At FG1, SSC variability during storms was assumed to be caused by landslides or channel erosion (Fig. 6a). Anecdotal and field observations reported unusually high SSC at FG1 during 2013, possibly from landsliding during previous large storms (G. Poysky, pers. comm.). At FG2 and FG3, additional variability in the Q–SSC relationship was caused by changing sediment availability from quarrying operations and construction in the village. High SSC values observed downstream of the quarry (FG2) during low Q were caused by two mechanisms: (1) P that generated high SSC runoff

Table 6
Goodness-of-fit statistics for storm metric-SSY_{EV} relationships. Spearman correlation coefficients significant at $p < 0.01$.

Model	Spearman	r^2	RMSE (tons)	Intercept (α)	Slope (β)	BCF
P_{sum_Upper}	0.70	0.39	4.31	0.003	1.10	2.71
P_{sum_Total}	0.88	0.71	2.43	0.033	1.11	1.39
EI_Upper	0.48	0.18	5.48	0.001	0.97	4.38
EI_Total	0.73	0.55	2.98	0.001	1.32	2.00
Q_{sum_Upper}	0.91	0.83	2.15	0.000	1.65	1.42
Q_{sum_Total}	0.83	0.70	2.46	0.000	1.29	1.50
Q_{max_Upper}	0.90	0.79	2.36	0.398	1.51	2.12
Q_{max_Total}	0.80	0.67	2.59	2.429	1.41	1.49

but did not result in storms identified on the hydrograph, and (2) washing fine sediment into the stream during quarry operations.

Given the close proximity of the quarry to the stream, SSC at FG2 was highly influenced by mining activity like rock extraction, crushing, and/or hauling operations. During 2012, a common practice for removing fine sediment from crushed aggregate was to rinse it with water pumped from the stream. In the absence of retention structures the fine sediment was discharged directly to Faga'alu stream, causing high SSC during non-storm periods with no P in the preceding 24 h (solid symbols, Fig. 6b and c). In 2013 and 2014, riverine discharge of rinsed sediment was discontinued, and sediment was piled on-site where erosion of these changing stockpiles caused high SSC only during storm events.

5.1.2. Compare SSY_{EV} with other kinds of sediment disturbance

SSY at Faga'alu was 3.9× higher than the natural background. Studies in similar watersheds have documented one to several orders of magnitude increases in SSY from land use that disturbs a small fraction of the watershed area (Stock et al., 2010). Urbanization (construction-phase) and mining can increase SSY by two to three orders of magnitude in catchments of several km^2, exceeding yields from the most unstable, tectonically active natural environments of Southeast Asia (Douglas, 1996). In three basins on St. John, US Virgin Islands unpaved roads increased sediment yields by 3–9 times (Ramos-Scharrón and Macdonald, 2005). Disturbances at larger scales in other watersheds draining to coral reef have been similar to Faga'alu, such as the Great Barrier Reef (GBR) catchment (423,000 km^2) where SSY increased by a factor of 5.5× since European settlement (Kroon et al., 2012). Mining has been a major contributor of sediment in other watersheds on volcanic islands with steep topography and high precipitation, increasing sediment yields by 5–10 times in a watershed in Papua New Guinea (Hettler et al., 1997; Thomas et al., 2003). In contrast to other land disturbances like fire, logging, or urbanization where sediment disturbance decreases over time, the disturbance from mining is persistently high. Disturbance magnitudes are similar to the construction phase of urbanization (Wolman and Schick, 1967), or high-traffic unpaved roads (Reid and Dunne, 1984), but persist or even increase over time.

While unpaved roads are often a major sediment source in humid forested regions (Lewis et al., 2001; Ramos-Scharrón and Macdonald, 2005; Reid and Dunne, 1984), most roads in the urban area in Faga'alu were stabilized with aggregate and were not generating significant amounts of sediment. Other disturbances in Faga'alu included a few small agricultural plots, small construction sites and bare dirt on roadsides. Repeated surface disturbance at the quarry is a key process maintaining high rates of sediment generation.

Annual sSSY from the quarry was estimated to be approximately 6700 tons/km^2/yr (Eq. (6)). The quarry surfaces are comprised of haul roads, piles of overburden, and steep rock faces which can be described as a mix of unpaved roads and cutslopes. sSSY from cutslopes varies from 0.01 tons/km^2/yr in Idaho (Megahan, 1980) to 105,000 tons/km^2/yr in Papua New Guinea (Blong and Humphreys, 1982), so the sSSY ranges measured in this study are well within the ranges found in the literature.

5.2. Modeling SSY_{EV} with storm metrics

Similar to other studies, the highest correlations with SSY_{EV} at Faga'alu were observed for discharge metrics Q_{sum} and Q_{max} (Basher et al., 2011; Duvert et al., 2012; Fahey et al., 2003; Hicks, 1990; Rankl, 2004; Rodrigues et al., 2013). Given the high correlation coefficients between SSY_{EV} and Q_{max} in both watersheds, Q_{max} may be a promising predictor that integrates both precipitation and discharge processes in diverse watersheds.

In Faga'alu, SSY_{EV} was least correlated with the EI. Rodrigues et al. (2013) hypothesized that EI is poorly correlated with SSY_{EV} due to the effect of previous events on antecedent moisture conditions and in-channel sediment storage. Cox et al. (2006) found EI was more correlated with soil loss in an agricultural watershed than a forested watershed, and Faga'alu is mainly covered in dense forest. P was measured near the quarry (RG1), which may reflect precipitation characteristics more accurately in the Lower than the Upper watershed, and account for the lower correlation coefficients between SSY_{EV_Upper} and P_{sum} and EI. SSY_{Lower} was hypothesized to be generated by sheetwash and rill formation at the quarry and agricultural plots, whereas SSY_{Upper} was hypothesized to be

Table 7
Precipitation totals and estimates of Annual SSY and sSSY calculated using five different methods.

			Eq. (6)		
	P_{sum} model, Events in 2014	Q_{max} model, Events in 2014	Events in Table 2	Events in Table 4	All measured events
Precipitation					
mm (% of P_{EVann})	2770	2770	1004 (36%)	299 (11%)	3,457 (125%)
Annual SSY (tons/year)					
Upper	35	129	46	120	41
Lower	152	526	310	300	388
Lower_Quarry	–	–	–	150	–
Lower_Village	–	–	–	150	–
Total	187	655	360	420	428
Annual sSSY (tons/km^2/year)					
Upper	39	143	51	140	45
Lower	173	598	350	340	441
Lower_Quarry	–	–	–	560	–
Lower_Village	–	–	–	250	–
Total	105	368	200	240	241

from channel processes and mass wasting. Mass wasting can contribute large pulses of sediment which can be deposited near or in the streams and entrained at high discharges during later storm events.

The Q–SSC relationship (sediment rating curve) coefficients including the intercept (α) and slope (β) can be interpreted as a function of watershed characteristics (Asselman, 2000). Similarly, Rankl (2004) hypothesized that the intercept in the Q_{max}–SSY_{EV} relationship varied with sediment availability and erodibility. While slopes in log–log space can be compared directly (Duvert et al., 2012), intercepts must be plotted in similar units and normalized by watershed area. Most studies do not correct storm metric-SSY models for log-bias, as is suggested by Ferguson (1986) for Q–SSC relationships, so we calculated the bias correction factor separately from the intercept (Eq. (5)) to compare our model slopes and intercepts with these other studies. In five semi-arid to arid watersheds (2.1–1538 km^2) in Wyoming, United States, Q_{max}–SSY_{EV} relationship intercepts ranged from 111 to 4320 (Q_{max} in $m^3/s/km^2$, SSY_{EV} in Mg/km^2) (Rankl, 2004). In eight sub-humid to semi-arid watersheds (0.45–22 km^2), intercepts ranged from 25 to 5039 (Duvert et al., 2012). In Faga'alu, intercepts were 0.4 and 2.4 in the undisturbed and disturbed watersheds, respectively. These intercepts are 1–2 orders of magnitude lower than in Rankl (2004) and Duvert et al. (2012), suggesting that sediment availability is relatively low under natural and human-disturbed conditions in Faga'alu.

High slope values in the log–log plots (β coefficient) suggest that small increases in stream discharge correlate with large increases in sediment load due to the erosive power of the stream or the availability of new sediment sources at high Q (Asselman, 2000). Rankl (2004) assumed that the slope was a function of rainfall intensity on hillslopes and found that the slopes were not statistically different among watersheds and ranged from 1.07 to 1.29 in semi-arid Wyoming. In watersheds in Duvert et al. (2012), slopes ranged from 0.95 to 1.82, and from 1.06 to 2.45 in eighteen other watersheds (0.60–1538 km^2) in diverse geographical settings (Basher et al., 1997; Fahey and Marden, 2000; Hicks et al., 2009; Rankl, 2004; Tropeano, 1991). In Faga'alu, slopes were 1.51 and 1.41 in the undisturbed and disturbed watersheds, respectively. These slopes are consistent with the slopes in Rankl (2004) and Duvert et al. (2012), despite large differences in climate and land cover.

5.3. Estimation of annual SSY: comparison with other tropical islands

Sediment yield is highly variable among watersheds, but is generally controlled by climate, vegetation cover, and geology, with human disturbance playing an increasing role in the 20th century (Syvitski et al., 2005). Sediment yields in tropical Southeast Asia and high-standing islands between Asia and Australia range from ~10 tons/km^2/yr in the granitic Malaysian Peninsula to ~10,000 tons/km^2/yr in the tectonically active, steeply sloped island of Papua New Guinea (Douglas, 1996). Sediment yields from Faga'alu are on the lower end of the range, with sSSY of 45–143 tons/km^2/yr from the undisturbed Upper watershed, and 241–368 tons/km^2/yr from the disturbed Total watershed (estimated from Q_{max} model with bias correction and Eq. (6) with all events).

Milliman and Syvitski (1992) report high average sSSY (1000–3000 tons/km^2/yr) from watersheds (10–100,000 km^2) in tropical Asia and Oceania. Their regional models of sSSY as a function of basin size and maximum elevation were not corrected for log-transform bias, but predict only 13 tons/km^2/yr from watersheds with peak elevation 500–1000 m (highest point of Upper Faga'alu subwatershed is 653 m), and 68 tons/km^2/yr for max elevations of 1000–3000 (Table 8). Given the high vegetation cover and lack of human disturbance in the Upper subwatershed, sSSY is expected to be lower than watersheds presented in Milliman and Syvitski

Table 8
Annual Specific Suspended Sediment Yield (sSSY) from steep, volcanic islands in the tropical Pacific.

Location	Drainage area (km2)	Mean annual precipitation (mm)	sSSY range tons/km^2/yr	Reference
Faga'alu Upper	0.88		45–143	This study
Faga'alu Total	1.78	2.380–6,350 (varies with elevation)	241–368	This study
Kawela, Molokai	13.5	500–3,000 (varies with elevation)	394	Stock and Tribble (2010)
Hanalei, Kauai	60.04	500–9,500 (varies with elevation)	545 ± 128	Ferrier et al. (2013)
Hanalei, Kauai	48.4	2,000–11,000 (varies with elevation)	525	Stock and Tribble (2010)
Hanalei, Kauai	54.4	2,000–11,000 (varies with elevation)	140 ± 55	Calhoun and Fletcher (1999)
St. John, USVI[a]	3.5	1,300–1,400	18	Ramos-Scharrón and Macdonald (2007)
St. John, USVI	2.3	1,300–1,400	24	Nemeth and Nowlis (2001)
St. John, USVI	6	1,300–1,400	36	Nemeth and Nowlis (2001)
Oahu	10.4	1,000–3,800 (varies with elevation)	330 ± 130; 200 ± 100 (varies with method)	Hill et al. (1997)
Barro Colorado, Panama	0.033	2,623 ± 458	100–200	Zimmermann et al. (2012)
Fly River, PNG	76,000	up to 10,000	1,000–1,500	Milliman (1995)
Purari River, PNG	35,000		3,000	"
Milliman and Syvitski (1992) Model[a] $sSSY = cA^f$				
River system (Relief, m)	c	f	sSSY tons/km^2/yr	
High Mountain (>3000)	280	−0.54	Upper = 296 Total = 205	
South Asia/Oceania (1000–3000)	65	−0.46	Upper = 68 Total = 50	
Upland (500–1000)	12	−0.59	Upper = 13 Total = 9	

[a] A is watershed area (km^2); c and f are regression coefficients for region and maximum watershed elevation.

(1992), but sSSY from the forested Upper Faga'alu subwatershed (45–68 tons/km^2/yr) was approximately three to five times higher than the prediction from the Milliman and Syvitski (1992) model (13 tons/km^2/yr). There is large scatter around their model for smaller watersheds, and the Faga'alu data fall within the range of scatter (Figs. 5e and 6e in Milliman and Syvitski (1992)). Faga'alu is also a much smaller watershed and the study period was relatively short (3 years) compared to others included in their models.

SSY was measured from two disturbed Hawaiian watersheds which are physiographically similar though larger than Faga'alu: Hanalei watershed on Kauai ("Hanalei", 54 km^2), and Kawela watershed on Molokai ("Kawela", 14 km^2) (Table 8) (Ferrier et al., 2013; Stock and Tribble, 2010). Hanalei had slightly higher rainfall (3,866 mm/yr) than Faga'alu (3,247 mm/yr) but slightly lower SSC (mean 63 mg/L, maximum of 2750 mg/L) than the Total Faga'alu watershed (mean 148 mg/L, maximum 3500 mg/L) (Ferrier et al., 2013; Stock and Tribble, 2010). Kawela is drier than Faga'alu (P varies with elevation from 500 to 3,000 mm) and had much higher SSC (mean 3,490 mg/L, maximum 54,000 mg/L) than the Total Faga'alu watershed. SSY from Hanalei was 369 ± 114 tons/km^2/yr (Ferrier et al., 2013), which is higher than the undisturbed subwatershed in Faga'alu (45–143 tons/km^2/yr) but similar to the disturbed Lower (441–598 tons/km^2/yr) subwatersheds. Stock and Tribble (2010) estimated SSY from Kawela was 459 tons/km^2/yr, similar to the disturbed Lower Faga'alu watershed, but higher than the Total Faga'alu watershed (241–368 tons/km^2/yr). Overall, both Hawaiian watersheds have higher sSSY than Faga'alu, which is consistent with the low Q_{max}–SSY$_{EV}$ intercepts and suggests Faga'alu has relatively low erosion rates for a steep, volcanic watershed. Precipitation variability may contribute to the difference in SSY, so a more thorough comparison between Hanalei and Faga'alu would require a storm-wise analysis of the type performed here.

6. Conclusion

Human disturbance has increased sediment yield to Faga'alu Bay to 3.9× pre-disturbance levels. The human-disturbed subwatershed accounted for the majority (87%) of Total sediment yield, and the quarry (1.1% of watershed area) contributed about a third of Total SSY to the Bay. The anthropogenic impact on SSY$_{EV}$ may vary by storm magnitude, as documented in Pacific Northwest forests (Lewis et al., 2001), but the storm metric models developed here showed contradictory results. Q_{max} was a good predictor of SSY$_{EV}$ in both the disturbed and undisturbed watersheds, making it a promising predictor in diverse environments. The slopes of the Q_{max}–SSY$_{EV}$ relationships were comparable with other studies, but the model intercepts were an order of magnitude lower than intercepts from watersheds in semi-arid to semi-humid climates. This suggests that sediment availability is relatively low in the Faga'alu watershed, either because of the forest cover or volcanic rock type.

This study presents an innovative method to combine sampling and analysis to measure sediment contributions from key sources, estimate baseline annual sediment yields prior to management, and rapidly develop an empirical sediment yield model for a remote, data-poor watershed. While the instantaneous Q–SSC relationship showed large increases in SSC downstream of key sources, the hysteresis and interstorm variability meant that a single Q–SSC relationship could not be used to estimate sediment loading, which is common in many watersheds (Asselman, 2000; Stock and Tribble, 2010). From a management perspective, the event-wise approach was useful for determining change over space and time without the problem of interannual variability in precipitation or the need for continuous, multi-year monitoring in a remote area. This approach is less expensive than efforts to measure annual yields and can be rapidly conducted if mitigation or disturbance activities are already planned.

Acknowledgements

Funding for this project was provided by NOAA Coral Reef Conservation Program (CRCP) through the American Samoa Coral Reef Advisory Group (CRAG). Kristine Bucchianeri at CRAG and Susie Holst at NOAA CRCP provided significant support. Christianera Tuitele, Phil Wiles, and Tim Bodell at American Samoa Environmental Protection Agency (ASEPA) contributed valuable scientific and material support, and Fatima Sauafea-Leau and Hideyo Hattori at NOAA, provided on-island coordination with traditional local authorities. Dr. Mike Favazza provided critical logistical assistance in American Samoa. Robert Koch at the American Samoa Coastal Zone Management Program (ASCMP) and Travis Bock at ASEPA assisted in accessing historical geospatial and water quality data. Professor Jameson Newtson, Rocco Tinitali, and Valentine Vaeoso at American Samoa Community College (ASCC), Meagan Curtis and Domingo Ochavillo at American Samoa Department of Marine and Wildlife Resources (DMWR), Don and Agnes Vargo at American Samoa Land Grant, Christina Hammock at NOAA American Samoa Climate Observatory, and Greg McCormick at San Diego State University supported the field and laboratory work. George Poysky Jr., George Poysky III, and Mitch Shimisaki at Samoa Maritime Ltd. provided unrestricted access to the Faga'alu quarry, and historical operation information. Faafetai tele lava.

Supplementary material

Supplementary data associated with this article can be found in the online version at http://dx.doi.org/10.1016/j.jhydrol.2016.03.053.

References

Asselman, N.E.M., 2000. Fitting and interpretation of sediment rating curves. J. Hydrol. 234, 228–248. http://dx.doi.org/10.1016/S0022-1694(00)00253-5.

Basher, L., Hicks, D., Clapp, B., Hewitt, T., 2011. Sediment yield response to large storm events and forest harvesting, Motueka River, New Zealand. New Zeal. J. Mar. Freshw. Res. 45, 333–356. http://dx.doi.org/10.1080/00288330.2011.570350.

Basher, L.R., Hicks, D.M., Handyside, B., Ross, C.W., 1997. Erosion and sediment transport from the market gardening lands at Pukekohe, Auckland, New Zealand. J. Hydrol. 36, 73–95.

Bégin, C., Brooks, G., Larson, R.A., Dragićević, S., Ramos Scharrón, C.E., Coté, I.M., 2014. Increased sediment loads over coral reefs in Saint Lucia in relation to land use change in contributing watersheds. Ocean Coast. Manag. 95, 35–45. http://dx.doi.org/10.1016/j.ocecoaman.2014.03.018.

Blong, R.J., Humphreys, G.S., 1982. Erosion of road batters in Chim Shale, Papua New Guinea. Civ. Eng. Trans. Inst. Eng. Aust. CE24 1, 62–68.

Boning, C., 1992. Recommendations for use of retransformation methods in regression models used to estimate sediment loads ("The bias correction problem").

Bonta, J.V., 2000. Impact of coal surface mining and reclamation on suspended sediment in Three Ohio Watersheds. JAWRA J. Am. Water Resour. Assoc. 36, 869–887.

Brunner, G., 2010. HEC-RAS River Analysis System.

Calhoun, R.S., Fletcher, C.H., 1999. Measured and predicted sediment yield from a subtropical, heavy rainfall, steep-sided river basin: Hanalei, Kauai, Hawaiian Islands. Geomorphology 30, 213–226.

Cox, C.A., Sarangi, A., Madramootoo, C.A., 2006. Effect of land management on runoff and soil losses from two small watersheds in St Lucia. Land. Degrad. Dev. 17, 55–72. http://dx.doi.org/10.1002/ldr.694.

Craig, P., 2009. Natural History Guide to American Samoa. National Park of American Samoa, Pago Pago, American Samoa.

Dames, Moore, 1981. Hydrologic Investigation of Surface Water for Water Supply and Hydropower.

Douglas, I., 1996. The impact of land-use changes, especially logging, shifting cultivation, mining and urbanization on sediment yields in humid tropical Southeast Asia: a review with special reference to Borneo. IAHS-AISH Publ. 236, pp. 463–471.

Duan, N., 2016. Smearing estimate: a nonparametric retransformation method author (s): Naihua Duan Source: Journal of the American Statistical Association, vol. 78, No. 383 (Sep., 1983), pp. 605–610. Published by : Taylor & Francis, Ltd. on behalf of the Ame. J. Am. Stat. Assoc. 78, 605–610.

Duvert, C., Gratiot, N., 2010. Construction of the stage-discharge rating curve and the SSC-turbidity calibration curve in San Antonio Coapa 2009 hydrological season.

Duvert, C., Nord, G., Gratiot, N., Navratil, O., Nadal-Romero, E., Mathys, N., Némery, J., Regüés, D., García-Ruiz, J.M., Gallart, F., Esteves, M., 2012. Towards prediction of suspended sediment yield from peak discharge in small erodible mountainous catchments (0.45–22 km^2) of France, Mexico and Spain. J. Hydrol. 454–455, 42–55. http://dx.doi.org/10.1016/j.jhydrol.2012.05.048.

Fabricius, K.E., 2005. Effects of terrestrial runoff on the ecology of corals and coral reefs: review and synthesis. Mar. Pollut. Bull. 50, 125–146. http://dx.doi.org/10.1016/j.marpolbul.2004.11.028.

Fahey, B.D., Marden, M., 2000. Sediment yields from a forested and a pasture catchment, coastal Hawke's Bay, North Island, New Zealand. J. Hydrol. 39, 49–63.

Fahey, B.D., Marden, M., Phillips, C.J., 2003. Sediment yields from plantation forestry and pastoral farming, coastal Hawke's Bay, North Island, New Zealand. J. Hydrol. 42, 27–38.

Fallon, S.J., White, J.C., McCulloch, M.T., 2002. Porites corals as recorders of mining and environmental impacts: Misima Island, Papua New Guinea. Geochim. Cosmochim. Acta 66, 45–62.

Fenner, D., Speicher, M., Gulick, S., Aeby, G., Aletto, S.C., Anderson, P., Carroll, B.P., DiDonato, E.M., DiDonato, G.T., Farmer, V., Fenner, D., Gove, J., Gulick, S., Houk, P., Lundblad, E., Nadon, M., Riolo, F., Sabater, M.G., Schroeder, R., Smith, E., Speicher, M., Tuitele, C., Tagarino, A., Vaitautolu, S., Vaoli, E., Vargas-angel, B., Vroom, P., 2008. The state of coral reef ecosystems of American Samoa. In: The State of Coral Reef Ecosystems of the United States and Pacific Freely Associated States, pp. 307–351.

Ferguson, R.I., 1986. River loads underestimated by rating curves. Water Resour. Res. 22, 74–76. http://dx.doi.org/10.1029/WR022i001p00074.

Ferguson, R.I., Grieve, I.C., Harrison, D.J., 1991. Disentangling land use effects on sediment yield from year to year climatic variability. Sediment Stream Water Qual. Chang. Environ. Trends Explan. 203, 13–20.

Ferrier, K.L., Taylor Perron, J., Mukhopadhyay, S., Rosener, M., Stock, J.D., Huppert, K. L., Slosberg, M., 2013. Covariation of climate and long-term erosion rates across a steep rainfall gradient on the Hawaiian island of Kaua'i. Bull. Geol. Soc. Am. 125, 1146–1163. http://dx.doi.org/10.1130/B30726.1.

Fuka, D., Walter, M., Archibald, J., Steenhuis, T., Easton, Z., 2014. EcoHydRology.

Gellis, A.C., 2013. Factors influencing storm-generated suspended-sediment concentrations and loads in four basins of contrasting land use, humid-tropical Puerto Rico. Catena 104, 39–57. http://dx.doi.org/10.1016/j.catena.2012.10.018.

Gippel, C.J., 1995. Potential of turbidity monitoring for measuring the transport of suspended solids in streams. Hydrol. Process. 9, 83–97.

Gomi, T., Moore, R.D., Hassan, M.A., 2005. Suspended sediment dynamics in small forest streams of the Pacific Northwest. J. Am. Water Resour. Assoc.

Gray, A.B., Warrick, J.A., Pasternack, G.B., Watson, E.B., Goñi, M.A., 2014. Suspended sediment behavior in a coastal dry-summer subtropical catchment: effects of hydrologic preconditions. Geomorphology 214, 485–501. http://dx.doi.org/10.1016/j.geomorph.2014.03.009.

Gray, J.R., 2014. Measuring suspended sediment. In: Ahuja, S. (Ed.), Comprehensive Water Quality and Purification. Elsevier, pp. 157–204. http://dx.doi.org/10.1016/B978-0-12-382182-9.00012-8.

Gray, J.R., Glysson, G.D., Turcios, L.M., Schwarz, G.E., 2000. Comparability of Suspended-Sediment Concentration and Total Suspended Solids Data U.S. Geological Survey Water-Resources Investigations Report 00-4191. Reston, Va.

Harmel, R.D., Cooper, R.J., Slade, R.M., Haney, R.L., Arnold, J.G., 2006. Cumulative uncertainty in measured streamflow and water quality data for small watersheds. Trans. Am. Soc. Agric. Biol. Eng. 49, 689–701.

Harmel, R.D., Smith, D.R., King, K.W., Slade, R.M., 2009. Estimating storm discharge and water quality data uncertainty: a software tool for monitoring and modeling applications. Environ. Model. Softw. 24, 832–842.

Harrelson, C.C., Rawlins, C.L., Potyondy, J.P., 1994. Stream channel reference sites: an illustrated guide to field technique. USDA Forest Service General Technical Report RM-245. US Department of Agriculture, Fort Collins CO.

Henderson, G.W., Toews, D.A.A., 2001. Using sediment budgets to test the watershed assessment procedure in Southeastern British Columbia. In: Toews, D.A.A., Chatwin, S. (Eds.), Watershed Assessment in the Southern Interior of British Columbia. B.C. Ministry of Forests, Research Branch, Victoria, British Columbia, pp. 189–208.

Hettler, J., Irion, G., Lehmann, B., 1997. Environmental impact of mining waste disposal on a tropical lowland river system: a case study on the Ok Tedi Mine, Papua New Guinea. Miner. Depos. 32, 280–291. http://dx.doi.org/10.1007/s001260050093.

Hewlett, J.D., Hibbert, A.R., 1967. Factors affecting the response of small watershed to precipitation in humid areas. For. Hydrol., 275–279

Hicks, D.M., 1990. Suspended sediment yields from pasture and exotic forest basins, In: Proceedings of the New-Zealand Hydrological Society Symposium. Auckland, New Zealand.

Hicks, D.M., Hoyle, J., Roulston, H., 2009. Analysis of sediment yields within Auckland region. ARC Technical Report 2009/064. Prepared by NIWA for Auckland Regional Council.

Holst-Rice, S., Messina, A., Biggs, T.W., Vargas-Angel, B., Whitall, D., 2015. Baseline Assessment of Fagaʻalu Watershed: A Ridge to Reef Assessment in Support of Sediment Reduction Activities. NOAA Coral Reef Conservation Program, Silver Spring, MD.

Horsley-Witten, 2011. American Samoa Erosion and Sediment Control Field Guide.

Horsley-Witten, 2012. Post-Construction Stormwater Training Memorandum.

Kearns, R., 2013. Personal Communication.

Kinnell, P.I.A., 2013. Modelling event soil losses using the Q R EI 30 index within RUSLE2. Hydrol. Process. http://dx.doi.org/10.1002/hyp.

Koch, R.W., Smillie, G.M., 1986. Comment on "River Loads Underestimated by Rating Curves" by R.I. Ferguson. Water Resour. Res. 22, 2121–2122.

Kostaschuk, R.a., Terry, J.P., Raj, R., 2002. Suspended sediment transport during tropical-cyclone floods in Fiji. Hydrol. Process. 17, 1149–1164.

Kroon, F.J., Kuhnert, P.M., Henderson, B.L., Wilkinson, S.N., Kinsey-Henderson, A., Abbott, B., Brodie, J.E., Turner, R.D.R., 2012. River loads of suspended solids, nitrogen, phosphorus and herbicides delivered to the Great Barrier Reef lagoon. Mar. Pollut. Bull. 65, 167–181. http://dx.doi.org/10.1016/j.marpolbul.2011.10.018.

Latinis, D.K., Moore, J., Kennedy, J., 1996. Archaeological Survey and Investigations Conducted at the Faga'alu Quarry, Ma'oputasi County, Tutuila, American Samoa, February 1996: Prepared for George Poysky, Sr., Samoa Maritime, PO Box 418, Pago Pago, American Samoa, 96799. Archaeological Consultants of the Pacific Inc., Pupukea Rd., Haleiwa, HI 96712. p. 59–624.

Lewis, J., 1996. Turbidity-controlled suspended sediment sampling for runoff-event load estimation. Water Resour. Res. 32, 2299–2310.

Lewis, J., Mori, S.R., Keppeler, E.T., Ziemer, R.R., 2001. Impacts of Logging on Storm Peak Flows, Flow Volumes and Suspended Sediment Loads in Caspar Creek, CA. In: Land Use and Watersheds: Human Influence on Hydrology and Geomorphology in Urban and Forest Areas. p. 1–76.

McDougall, I., 1985. Age and evolution of the volcanoes of Tutuila American Samoa. Pacific Sci. 39, 311–320.

Megahan, W.F., 1980. Erosion from roadcuts in granitic slopes of the Idaho Batholith. In: Proceedings Cordilleran Sections of the Geological Society of America, 76th Annual Meeting. Oregon State University, Corvallis, OR, p. 120.

Megahan, W.F., Wilson, M., Monsen, S.B., 2001. Sediment production from granitic cutslopes on forest roads in Idaho, USA. Earth Surf. Process. Landforms 26, 153–163.

Milliman, J.D., 1995. Sediment discharge to the ocean from small mountainous rivers: the New Guinea example. Geo-Mar. Lett. 15 (3–4), 127–133.

Milliman, J.D., Syvitski, J.P.M., 1992. Geomorphic/tectonic control of sediment discharge to the ocean: the importance of small mountainous rivers. J. Geol. 100, 525–544.

Minella, J.P.G., Merten, G.H., Reichert, J.M., Clarke, R.T., 2008. Estimating suspended sediment concentrations from turbidity measurements and the calibration problem. Hydrol. Process. 22, 1819–1830. http://dx.doi.org/10.1002/hyp.6763.

Nakamura, S., 1984. Soil Survey of American Samoa. US Department of Agriculture Soil Conservation Service, Pago Pago, American Samoa.

Nathan, R.J., McMahon, T.A., 1990. Evaluation of automated techniques for base flow and recession analyses. Water Resour. Res. 26, 1465–1473. http://dx.doi.org/10.1029/WR026i007p01465.

Nearing, M.A., Nichols, M.H., Stone, J.J., Renard, K.G., Simanton, J.R., 2007. Sediment yields from unit-source semiarid watersheds at Walnut Gulch. Water Resour. Res. 43, 1–10. http://dx.doi.org/10.1029/2006WR005692.

Nemeth, R.S., Nowlis, J.S., 2001. Monitoring the effects of land development on the near-shore reef environment of St. Thomas, USVI. Bull. Mar. Sci. 69 (2), 759–775.

Perreault, J., 2010. Development of a Water Budget in a Tropical Setting Accounting for Mountain Front Recharge. University of Hawai'i, Tutuila, American Samoa.

Perroy, R.L., Bookhagen, B., Chadwick, O.a., Howarth, J.T., 2012. Holocene and anthropocene landscape change: Arroyo Formation on Santa Cruz Island, California. Ann. Assoc. Am. Geogr. 102, 1229–1250. http://dx.doi.org/10.1080/00045608.2012.715054.

Ramos-Scharrón, C.E., Macdonald, L.H., 2005. Measurement and prediction of sediment production from unpaved roads, St John, US Virgin Islands. Earth Surf. Process. Landforms 30, 1283–1304.

Ramos-Scharrón, C.E., Macdonald, L.H., 2007. Measurement and prediction of natural and anthropogenic sediment sources, St. John, US Virgin Islands. Catena 71, 250–266.

Rankl, J.G., 2004. Relations Between Total-Sediment Load and Peak Discharge for Rainstorm Runoff on Five Ephemeral Streams in Wyoming. U.S. Geological Survey Water-Resources Investigations Report 02-4150. Denver, CO.

Rapp, A., 1960. Recent development of mountain slopes in Karkevagge and surroundings, northern Scandinavia. Geogr. Ann. 42, 65–200.

Reid, L.M., Dunne, T., 1984. Sediment production from forest road surfaces. Water Resour. Res. 20, 1753–1761.

Reid, L.M., Dunne, T., 1996. Rapid Evaluation of Sediment Budgets. Catena Verlag, Reiskirchen, Germany.

Risk, M.J., 2014. Assessing the effects of sediments and nutrients on coral reefs. Curr. Opin. Environ. Sustain. 7, 108–117. http://dx.doi.org/10.1016/j.cosust.2014.01.003.

Rodrigues, J.O., Andrade, E.M., Ribeiro, L.A., 2013. Sediment loss in semiarid small watershed due to the land use. Rev. Ciência Agronômica 44, 488–498.

Rotmann, S., Thomas, S., 2012. Coral tissue thickness as a bioindicator of mine-related turbidity stress on coral reefs at Lihir Island, Papua New Guinea. Oceanography 25, 52–63.

Sadeghi, S.H.R., Mizuyama, T., Miyata, S., Gomi, T., Kosugi, K., Mizugaki, S., Onda, Y., 2007. Is MUSLE apt to small steeply reforested watershed? J. For. Res. 12, 270–277. http://dx.doi.org/10.1007/s10310-007-0017-9.

Slaymaker, O., 2003. The sediment budget as conceptual framework and management tool. Hydrobiologia 494, 71–82.

Stock, J.D., Rosener, M., Schmidt, K.M., Hanshaw, M.N., Brooks, B.A., Tribble, G., Jacobi, J., 2010. Sediment budget for a polluted Hawaiian reef using hillslope monitoring and process mapping. In: American Geophysical Union Fall Meeting. p. #EP22A-01.

Stock, J.D., Tribble, G., 2010. Erosion and sediment loads from two Hawaiian watersheds. In: 2nd Joint Federal Interagency Conference. Las Vegas, NV.

Storlazzi, C.D., Norris, B.K., Rosenberger, K.J., 2015. The influence of grain size, grain color, and suspended-sediment concentration on light attenuation: Why fine-grained terrestrial sediment is bad for coral reef ecosystems. Coral Reefs 34, 967–975. http://dx.doi.org/10.1007/s00338-015-1268-0.

Syvitski, J.P.M., Vörösmarty, C.J., Kettner, A.J., Green, P., 2005. Impact of humans on the flux of terrestrial sediment to the global coastal ocean. Science 308, 376–380. http://dx.doi.org/10.1126/science.1109454 (80-).

Thomas, S., Ridd, P.V., Day, G., 2003. Turbidity regimes over fringing coral reefs near a mining site at Lihir Island, Papua New Guinea. Mar. Pollut. Bull. 46, 1006–1014. http://dx.doi.org/10.1016/S0025-326X(03)00122-X.

Tonkin & Taylor International Ltd., 1989. Hydropower Feasibility Studies Interim Report – Phase 1. Ref: 97/10163.

Topping, J., 1972. Errors of Observation and their Treatment, fourth ed. Chapman and Hall, London, UK.

Tropeano, D., 1991. High flow events, sediment transport in a small streams in the "Tertiary Basin" area in Piedmont (northwest Italy). Earth Surf. Process. Landforms 16, 323–339.

Turnipseed, D.P., Sauer, V.B., 2010. Discharge Measurements at Gaging Stations, in: U.S. Geological Survey Techniques and Methods Book 3, Chap. A8. Reston, Va., pp. 87.

URS Company, 1978. American Samoa Water Resources Study: Assessment of Water Systems American Samoa. Coastal Zone Information Center, Honolulu, HI.

USGS, NRTWQ, 2016. Methods for Computing Water Quality Using Regression Analysis [WWW Document]. <http://nrtwq.usgs.gov/md/methods/> (accessed 03.01.16).

Walling, D.E., 1977. Assessing the accuracy of suspended sediment rating curves for a small basin. Water Resour. Res. 13, 531–538.

Walling, D.E., 1999. Linking land use, erosion and sediment yields in river basins. Hydrobiologia 410, 223–240.

Walling, D.E., Collins, A.L., 2008. The catchment sediment budget as a management tool. Environ. Sci. Policy 11, 136–143. http://dx.doi.org/10.1016/j.envsci.2007.10.004.

Walling, D.E., Webb, B.W., 1996. Erosion and sediment yield: a global overview. Eros. Sediment Yield Glob. Reg. Perspect. Proceeedings Exet. Symp., pp. 3–19.

Wemple, B.C., Jones, J.A., Grant, G.E., 1996. Channel network extension by logging roads in two basins, Western Cascades, Oregon. Water Resour. Bull. 32, 1195–1207.

Wolman, M.G., Schick, A.P., 1967. Effects of construction on fluvial sediment, urban and suburban areas of Maryland. Water Resour. Res. 3, 451–464.

Wong, M., 1996. Analysis of Streamflow Characteristics for Streams on the Island of Tutuila, American Samoa. U.S. Geological Survey Water-Resources Investigations Report 95-4185.

Wulf, H., Bookhagen, B., Scherler, D., 2012. Climatic and geologic controls on suspended sediment flux in the Sutlej River Valley, western Himalaya. Hydrol. Earth Syst. Sci. 16, 2193–2217. http://dx.doi.org/10.5194/hess-16-2193-2012.

Zimmermann, A., Francke, T., Elsenbeer, H., 2012. Forests and erosion: Insights from a study of suspended-sediment dynamics in an overland flow-prone rainforest catchment. J. Hydrol., 170–181